Quaternary Geochronology 65 (2021) 101185

Contents lists available at ScienceDirect

Quaternary Geochronology

journal homepage: www.elsevier.com/locate/quageo

A multi-method dating approach to reassess the geochronology of faulted Quaternary deposits in the central sector of the Iberian Chain (NE Spain)

Davinia Moreno [a,*], Francisco Gutiérrez [b], Miren del Val [a,c], Domingo Carbonel [b], Fernando Jiménez [a,d], M Jesús Alonso [a], Virginia Martínez-Pillado [e,a], Oswaldo Guzmán [f,a], Gloria I. López [g,a], David Martínez [a]

[a] Centro Nacional de Investigación sobre la Evolución Humana (CENIEH), Paseo Sierra de Atapuerca 3, 09002, Burgos, Spain
[b] Departamento de Ciencias de la Tierra, Universidad de Zaragoza. Calle Pedro Cerbuna 12, 50009, Zaragoza, Spain
[c] Departamento de Mineralogía y Petrología, Facultad de Ciencia y Tecnología, Universidad del País Vasco. Barrio Sarriena s/n, 48940, Leioa, Bizkaia, Spain
[d] Departamento de Química Analítica, Facultad de Ciencias, Universidad de Valladolid. Campus Miguel Delibes, Paseo de Belén 7, 47011, Valladolid, Spain
[e] Centro Mixto UCM-ISCIII. Av. Monforte de Lemos 5, pabellón 14, 28029, Madrid, Spain
[f] Grupo de Investigación en Ciencias de la Tierra y Clima, Universidad Regional Amazónica Ikiam, Parroquia Muyuna, km 7 vía a Alto Tena, Ecuador
[g] Leon Recanati Institute for Maritime Studies RIMS, University of Haifa. 199 Aba Khoushy Ave, Mt Carmel, Haifa, 3498838, Israel

ARTICLE INFO

Keywords:
ESR dating
OSL dating
U-series dating
Radiocarbon dating
Fluvial terraces
Paleoseismology
Seismic hazard

ABSTRACT

Seismic hazard assessment and geochronology are closely linked disciplines. The quantity and quality of the geochronological data used for fault-source characterization is crucial in seismic hazard estimates, which may have significant socio-economic implications. The characterization of Quaternary faults in the central sector of the Iberian Chain (NE Spain) has traditionally been based on ages provided by a now closed commercial luminescence laboratory. In this work, we compare new geochronological data obtained by a multi-method dating approach from pediment and terraces (Electron Spin Resonance: ESR, Optically Stimulated Luminescence: OSL; U-series: U/Th) and short-transport colluvial facies (radiocarbon), with ages provided by the commercial luminescence lab from the same units. The thirteen new numerical ages from terraces and pediments associated with Quaternary faults are systematically 6–3 times older than the previous ones, strongly suggesting that they lead to significant overestimates of fault activity and seismic hazard in the region. These new ESR, OSL and U/Th ages and the lack of information about the methodology applied by the closed luminescence laboratory seriously question the reliability of the previous ages. It also highlights the need of revisiting the Quaternary and geomorphological studies carried out in Spain using non-reliable ages.

1. Introduction

Geochronology is an essential tool in tectonic geomorphology and paleoseismological studies aimed at characterizing fault sources for seismic hazard assessment. The quality and interpretation of the geochronological data used for fault-source characterization may have a critical impact in seismic hazard estimates with significant socio-economic implications (e.g., feasibility of major engineering projects, cost of seismic-resistant designs). The condition of a tectonic fault as active according to most regulatory definitions is based on chronological criteria, i.e., whether the fault has experienced any displacement event after an established chronological bound. Inaccurate ages or with high error margins may lead to erroneous or indeterminate ascriptions. For instance, if the time span considered in the regulatory definition is 35 ka and the geochronological data indicate that the most recent displacement on a fault occurred sometime within the 40–30 ka time span, the epistemic uncertainty associated with the geochronological information would lead to an indeterminate situation (see discussion in Carbonel et al., 2019; McCalpin, 2009).

Some of the most important parameters used to assess the seismogenic potential of faults are based on geochronological data (e.g., McCalpin, 2009): fault slip rate, earthquake recurrence and timing of paleoearthquakes, especially the Most Recent Event (MRE). The slip rate can be estimated dividing the cumulative displacement of an offset geomorphic or stratigraphic marker across a fault, by its numerical age (neotectonic or long-term slip rate; Burbank and Anderson, 2012). It can

* Corresponding author.
E-mail address: davinia.moreno@cenieh.es (D. Moreno).

https://doi.org/10.1016/j.quageo.2021.101185
Received 23 June 2020; Received in revised form 14 April 2021; Accepted 15 April 2021
Available online 12 May 2021
1871-1014/© 2021 Elsevier B.V. All rights reserved.

also be calculated dividing the displacement of one or more dated paleoearthquakes by the time span of the corresponding closed seismic cycles (closed-cycle or paleoseismic slip rate). Earthquake recurrence can be derived directly from numerically dated and complete paleoseismic histories, and indirectly from slip rates, considering that earthquake frequency is related to the rate at which energy is accumulated in a fault through elastic strain (Young and Coppersmith, 1985). Paleoseismologists seek for the best approximation to the timing of each paleoearthquake. In an ideal situation, the age of a specific stratigraphic unit could allow resolving the timing of a paleoearthquake if the deposit was accumulated during or soon after the earthquake (e.g., coseismic rock avalanche, colluvial wedge). Most frequently, the age of paleoearthquakes is constrained by dating sediments or landforms formed before and after the event (i.e., maximum and minimum bracketing ages) (McCalpin, 2009). Of particular interest is the age of the MRE, since the probability of the next large earthquake on a fault depends on the time elapsed since the last rupture event (i.e., renewal or conditional probability models).

Close collaboration and mutual support between paleoseismologists and geochronologists are essential for the proper assessment of the seismogenic hazard associated with active tectonic faults (McCalpin, 2009; Sowers et al., 1998). In an initial phase, decisions on the most appropriate dating method for each site and its multiple targeted morpho-stratigraphic features should be based on a good understanding of the geological and geomorphological contexts, as well as the assumptions, requirements and limitations associated with the different geochronological techniques. Nevertheless, the application of multiple dating methods is highly recommended, since it is unlikely that a robust chronology can be established using a single dating method. It also allows cross-checking the validity of the available numerical ages, identifying potential systematic biases and taking decisions about anomalous ages (e.g., age reversals, age outliers) (McCalpin, 2009; Sowers et al., 1998).

A potential problem that may arise from the application of multiple methods is elucidating which ages are the most reliable ones when the results of the different techniques show significant inconsistencies. The decision to disregard one or more samples should be based not only on the analytical data, but also on the available information on the study area (geological, geomorphological, pedological, paleoenvironmental, paleontological, archaeological). Apparent inconsistencies between numerical ages may also contribute to better understand complex stratigraphic and structural relationships. For instance, OSL ages from a trench dug in Ragged Mountain Thrust (Alaska) helped to resolve whether a steep and sharp contact was a secondary fault or a paleochannel margin (McCalpin et al., 2020). Apart from that, absolute dendrochronology dates obtained at the Hazel Dell paleoseismic site of the San Andreas Fault showed that detrital charcoal used to constrain the age of paleoearthquakes is systematically older (ca. 322 a) than the deposit that contains it (i.e. detrital charcoal is charred before deposition) (Streig et al., 2020). Thanks to this correction it was determined that two historic Bay Area earthquakes ruptured the surface in 1838 and 1890 instead of 1700 or earlier as previously proposed.

This work presents and discusses a multi-method investigation conducted for the reassessment of the geochronology of Quaternary deposits associated with slow-moving seismogenic faults in the intraplate Iberian Chain, NE Spain. In this area, most of the previously existing geochronological data correspond to TL ages provided by the now closed *Laboratorio de Datación y Radioquímica de la Universidad Autónoma de Madrid* (UAM Luminescence Lab) in reports with exiguous details on the analytical methods (Gutiérrez et al., 2020a, 2020b, 2009, 2008; Simón et al., 2017 and references therein). Our aim in this study is to evaluate the validity of those previous TL ages by applying different dating methods such as Electron Spin Resonance (ESR), Optically Stimulated Luminescence (OSL), Uranium–Thorium (U/Th) series and radiocarbon dating (^{14}C), in some cases replicating samples previously analyzed at the UAM Luminescence Lab. The selection of the dating method for each unit was based on the nature and origin of the deposits and their relative chronology, mainly based on previous geomorphological maps that establish the terrace and pediments sequences (Gutiérrez, 1998).

The new geochronological data presented in this work seriously challenge the validity of the previous TL ages that seem to significantly overestimate the activity of the faults (Gutiérrez et al., 2020b), potentially leading to substantial seismic hazard overestimates with societal implications (e.g., interruption and re-design of Teruel Hospital; Simón et al., 2016).

2. Quaternary faults in the central sector of the Iberian Chain

The Iberian Chain in NE Spain is an intraplate orogen generated in late Cretaceous to Miocene times during the Alpine contraction (Guimerà, 2018). This orogenic phase, which caused the tectonic inversion of Mesozoic extensional basins, was related to the compressional stress field developed within the Iberian microplate as a result of the convergence between the African and European plates (De Vicente et al., 2005). Around the Middle Miocene, the stress regime changed from compressional into extensional, starting the currently active post-orogenic phase (Gutiérrez et al, 2008, 2012; Simón et al., 2012). Crustal extension is attributed to the development of the Valencia Trough in the western Mediterranean. Two generations of neotectonic grabens can be differentiated on the basis of cartographic relationships.

The *first graben-formation phase* produced the largest intramontane basins in the central sector of Iberian Chain: the Calatayud Graben and the Teruel Graben, both around 100 km long and filled with Mio-Pliocene terrestrial sediments several hundred meters thick (Fig. 1). Locally, the top of the endorheic fill of these basins corresponds to Pliocene lacustrine limestones that constitute useful markers to assess the long-term activity of some Quaternary faults. The *second graben-formation phase*, initiated in the Late Pliocene, produced new extensional basins that cross-cut and/or are inset with respect to the pre-existing Teruel and Calatayud basins. From south to north these include: the Jiloca neotectonic depression (Cortés Gracia and Casas-Sainz, 1996; Gracia et al., 2003; Rubio and Simón, 2007; Simón et al, 2016, 2017), the Daroca Half-graben (Gracia Prieto, 1992; Gutiérrez et al., 2020a), the Munébrega Half-graben (Gutiérrez et al., 2009) and the Río Grío Graben (Gutiérrez et al., 2013) (Fig. 1).

The development of the drainage network in the central sector of the Iberian Chain has been controlled by the episodic formation of NW-SE to NNE-SSW oriented grabens, and their progressive capture and change from endorheic to exorheic conditions (Gutiérrez et al., 2008). The fluvial systems have developed stepped sequences of mantled pediments and terraces which constitute the main morpho-stratigraphic markers used to characterize the activity and seismogenic potential of the Quaternary faults. The fluvial network is dominated by longitudinal drainages subparallel to the basin-bounding faults (Fig. 1). In these situations, fault activity is mainly recorded in marginal mantled pediments and alluvial fans. However, where the faults are crossed by transverse drainages, fault displacement is mainly recorded by fluvial terraces (e.g. Alfambra River that traverses the Concud Fault).

2.1. Jiloca neotectonic depression

The NNW-SSE oriented and 70 km-long Jiloca neotectonic depression is controlled on its eastern margin by three major NW-SE to N–S trending normal faults with a right stepping en echelon arrangement, from north to south: Calamocha Fault, Palomera Fault, and Concud-Teruel Fault (Gutiérrez et al., 2012; Simón et al., 2012) (Fig. 1). The Calamocha Fault and the Teruel-Concud Fault offset vertically around 200–250 m Pliocene limestones of the adjacent Calatayud and Teruel basins, respectively. The latter fault comprises two segments separated by a step over 1.5 km wide, traditionally designated as Concud Fault and Teruel Fault. This work addresses the chronology of Quaternary deposits at three sites associated with the Concud Fault (BA: Los Baños; CO:

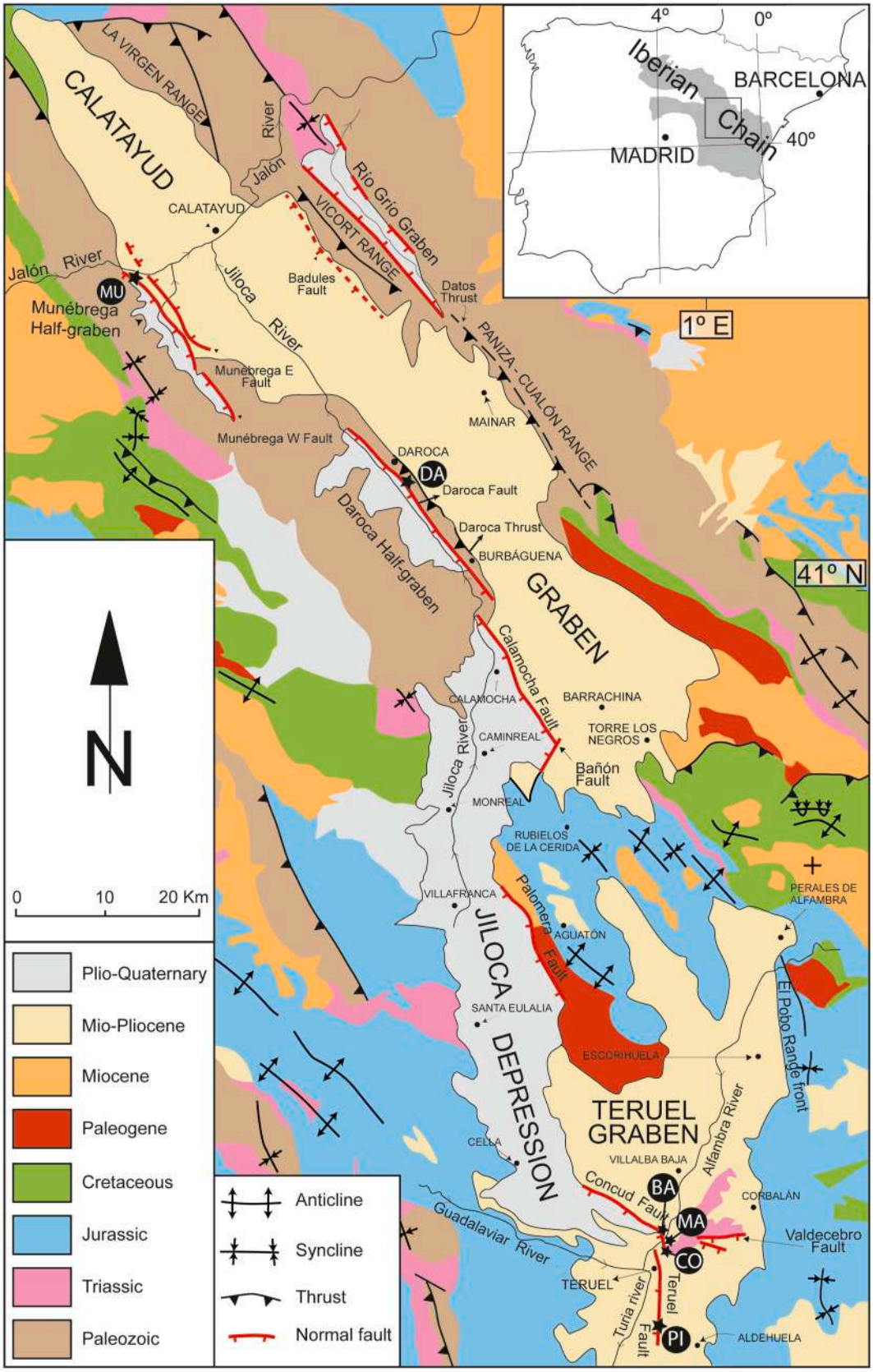

Fig. 1. Geological map of the central sector of the Iberian Chain showing the location of the main Quaternary faults and the sampling sites (Modified from Gutiérrez et al., 2020b). MU: Munébrega W Fault; DA: Daroca Fault; BA: Los Baños; MA: Mataueta; CO: Cociero; PI: Pitarque.

Cociero; MA: Mataueta) and one site of the Teruel Fault (PI: Pitarque), briefly described below.

2.1.1. Concud Fault

2.1.1.1. Los Baños site. Concud Fault is exposed at the old railway trench of Los Baños, located on the western margin of the Alfambra River valley (Figs. 1 and 2). In the footwall, the Upper Miocene bedrock is unconformably overlain by a terrace of the Alfambra River, perched 60–66 m above the current channel. This terrace deposit consists of a lower unit of cemented gravels with interbedded fine-grained beds and an indurated upper tufa unit up to 7 m thick. This tufa unit was previously dated by U/Th series in two laboratories: Recherches Appliquées au Karst, Faculté Polytechnique de Mons in Belgium (Arlegui et al, 2005, 2006) and McMaster University in Canada (Gutiérrez et al., 2008) (See Section 3 and Table 1). The exposed section of the downthrown block shows two sedimentary packages (PI and PII in Fig. 2) bounded by an angular unconformity, and three overlapping fissures abutting the fault plane and filled by colluvial facies (FF1, FF2 and FF3 in Fig. 2). The strongly deformed package PI consists of sands (I1), conglomerates (I2), a layer of calcareous tufa (I3), and silts (I4) (Fig. 2). Beds of fine-grained detrital facies situated in units I4 and I1 were previously dated at the UAM Luminescence Laboratory (See Section 3 and Table 1). The less deformed upper package PII is made up of colluvial deposits interdigitated away from the fault with relatively well-sorted alluvial deposits.

2.1.1.2. Cociero site. Cociero site is a road-cut exposure located on the eastern margin of the Alfambra valley (Fig. 3). Here, a terrace deposit situated at approximately 19 m above the channel is offset 1.7–2.2 m by a fault. This fault, at some distance from the main strand of Concud Fault, has been attributed to a secondary tectonic rupture (Lafuente et al., 2011) while other authors indicate that it could be also related to dissolution of underlying Triassic evaporites (Gutiérrez et al., 2012). The fault is truncated by non-deformed colluvial deposits.

2.1.1.3. Mataueta site. Mataueta site, also located on the eastern margin of the Alfambra River valley, corresponds to a pediment deposits offset on its proximal sector by Concud Fault, as revealed by a trench investigated by Ezquerro et al. (2014) and Simón et al. (2016) (Fig. 4).

2.1.2. Teruel Fault

2.1.2.1. Pitarque site. Pitarque site corresponds to a section of the Valdelobos stream, a tributary of the Turia River, which transversally crosses the trace of the Teruel Fault (Figs. 1 and 5). Here, a terrace of the Valdelobos Stream, perched around 60 m above the thalweg, is offset vertically 8–9.5 m by the Teruel Fault (Gutiérrez et al., 2020b; Simón et al., 2017). Two paleoseismological trenches excavated in a remnant of this terrace on the downthrown block were investigated by Simón et al. (2017).

2.2. Daroca half-graben

The NW-SE trending Daroca Half-graben is controlled on its NE margin by the SW-dipping and 27 km long Daroca Fault (Figs. 1 and 6). This asymmetric basin is inset with respect to the Calatayud Basin and drained longitudinally by the Jiloca River. The best exposure of the fault is located in a quarry situated 1.5 km south of Daroca town, where the fault clearly ruptures a mantled pediment perched at the site 35 m above the Jiloca River.

2.3. Munébrega half-graben

The 19 km long and NW-SE trending Munébrega Half-graben is superimposed on and inset into the Calatayud Basin along its southwestern margin, just south of the transverse Jalón River valley. This Plio-Quaternary basin is controlled on its NE margin by the Munébrega W Fault, which has offset a mantled pediment and generated an uphill-facing scarp 6–7 m high (Fig. 7). The faulted pediment merges with a terrace of the Jalón River perched 45 m above the current channel. Gutiérrez et al. (2009) investigated a paleoseismological trench excavated across the antislope fault scarp.

3. Previous geochronology

The number of neotectonic and paleoseismological investigations in the central sector of the Iberian Chain has experienced a great increase since the first work that started to use luminescence dating (Gutiérrez et al., 2008). Previously, numerical chronological data were very restricted, hampering the quantitative assessment of the activity and seismogenic potential of the faults. Burillo et al. (1985) roughly dated a faulted colluvium on the western margin of the Jiloca graben using some fragments of ceramics found among the sediments. The typology of these archaeological remains indicated an age between 1200- and 500-years BC, after the Middle Bronze Age and before the Iberian culture. Arlegui et al. (2006, 2005) dated the tufa deposits capping the footwall terrace at Los Baños site using two U/Th series ages of 169 ± 10 and 116 ± 4 ka (Fig. 2 and Table 1). In a later work, Simón et al. (2005) postulated that this tufa deposits (ca. 7 m thick) are correlative to a much thinner tufa layer (<0.5 m thick) in the downthrown block (unit I3 of package PI in Fig. 2) and estimated a long-term slip rate of 0.23–0.59 mm/a for Concud Fault considering the displacement and the U/Th ages (Arlegui et al., 2005). The rest of the available long-term slip rates by that time were mainly based on the displacement of biostratigraphically-dated Pliocene limestones, indicating slip rates of the order of 0.05–0.1 mm/a (Gutiérrez, 1998; Gutiérrez et al., 2008).

Most of the recent investigations on Quaternary faults in the Iberian Chain rely on ages provided by the now closed *Laboratorio de Datación y Radioquímica de la Universidad Autónoma de Madrid* (UAM Luminescence Lab): Munébrega Fault (Gutiérrez et al., 2009), Daroca Fault (Gutiérrez et al., 2008), Calamocha Fault (Martín-Bello et al., 2014), Concud Fault at Los Baños site (Gutiérrez et al., 2008; Lafuente et al., 2011), Cociero site (Gutiérrez et al., 2008; Lafuente, 2011; Lafuente et al., 2011), Matauetа site (Ezquerro et al., 2014; Simón et al., 2016), Hocino site (backfilled trenches; Lafuente et al., 2014, 2011), and Teruel Fault at Pitarque site (Simón et al, 2012, 2017). These ages obtained by TL dating are presented in Table 1. As discussed in Gutiérrez et al. (2020b), from these luminescence ages, can be calculated: (1) long-term slip rates significantly higher than those inferred from the Pliocene limestones (e.g. Concud Fault 0.29 mm/a vs. 0.1 mm/a); (2) average earthquake recurrence values much higher than those estimated for other normal faults in intraplate Spain; (3) anomalously high fluvial-incision rates derived from the ages of perched terraces. These features suggested that the luminescence ages obtained through a scarcely known approach by the UAM Luminescence Lab were probably underestimating the actual ages of the deposits and overestimating the seismic hazard of the associated faults. Unfortunately, numerical ages obtained by other methods and by other laboratories were very scarce, limiting our capability to assess the reliability of the ages provided by the UAM Luminescence Lab. In the Rubielos de la Cérida Fault, a 2.5 km long fault located in the transfer zone between the Calamocha and Palomera faults, Gutiérrez et al. (2008) estimated a vertical slip rate of 0.05–0.07 mm/a based on radiocarbon ages and comparable with the values obtained for other faults using as markers the Pliocene limestones. A recent work on the Valdecebro Fault (Teruel Neogene Graben; Fig. 1), based on OSL ages from the laboratory of the Radioisotopes Unit at the University of Seville (Spain), indicates a long-term slip rate for this fault of 0.05 mm/a (Simón et al., 2019), also significantly lower than those obtained with the luminescence ages of the UAM Luminescence Lab.

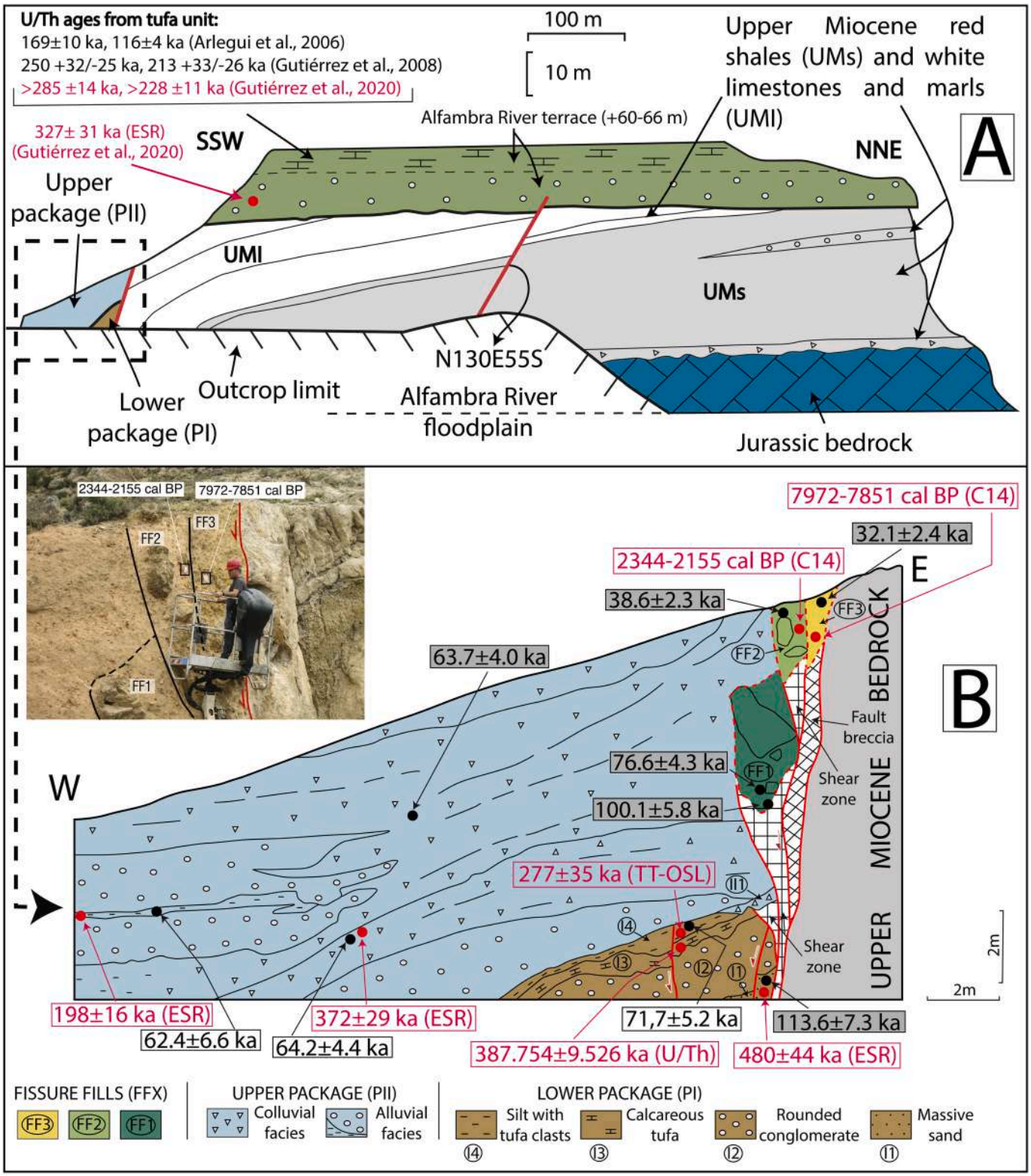

Fig. 2. Sketches illustrating the main stratigraphic and structural relationships associated with the Concud Fault exposed at Los Baños site. (A) General section showing the main units exposed on both sides of the faults. (B) Sketch and photograph showing the Quaternary deposits in the downthrown block, including two unconformable packages and three nested fissure fills abutting the fault plain. Previous ages provided by the UAM Luminescence Lab are indicated in white (Gutiérrez et al., 2008) and grey boxes (Lafuente et al., 2011). New ages are indicated with red characters: Electron Spin Resonance (ESR); Optically Stimulated Luminescence (OSL); AMS radiocarbon (^{14}C); Uranium series (U/Th). Modified after (Gutiérrez et al., 2020b)

Table 1
Comparison of the previous geochronological framework and the new ages presented in this work in the central sector of the Iberian Chain.

Fault	Site	Level	Unit	Sample	CENIEH Lab ages (ka)	Dating method	Previous ages (ka)	Dating method	References
Concud	**Los Baños**	Upper Package (PII)		T-BAN1705	198 ± 16	ESR	62,4 ± 6,6	TL	(Gutiérrez et al., 2008, 2020a; Lafuente et al., 2010, 2011)
				T-BAN1704	372 ± 29	ESR	64,2 ± 4,4		
					No new age		63,7 ± 4,0		
		Lower Package (PI)	I4	T-BAN1703	277 ± 35	TT-OSL	71,7 ± 5,2	TL	
			I3	T-BA-SU-3	388 ± 10	U/Th	No previous age		
			I1	T-BAN1701	480 ± 44	ESR	113,6 ± 7,3	TL	
		Fissure Fills	FF3	T-BAN1706	7972 - 7851 cal BP	^{14}C	32,1 ± 2,4	TL	
			FF2	T-BAN1707	2344 - 2155 cal BP	^{14}C	38,6 ± 2,3		
			FF1		No new age		76,6 ± 4,8		
							100,1 ± 5,8		
		Terrace (alluvium)		T-BAN1708	327 ± 31	ESR	No previous age		
		Terrace (tufa unit)		T-BA-SU-1	>285 ± 14	U/Th	169 ± 10	U/Th	(Arlegui et al., 2006; Gutiérrez et al., 2008, 2020a)
							116 ± 4		
				T-BA-SU-2	>228 ± 11		250 + 32/-25		
							213 + 33/-26		
	Mataueta	Pediment deposits		T-MAT1714	87 ± 3	OSL	21,3 ± 1,5	TL	(Ezquerro et al., 2014; Gutiérrez et al., 2020a; Simón et al., 2016)
							21,0 ± 1,3		
							21,1 ± 1,4		
							19,2 ± 1,2		
							16,4 ± 1,2		
							12,8 ± 0,7		
							27,6 ± 1,4		
							17,2 ± 1,2		
							14,2 ± 0,8		
							18,8 ± 1,2		
	Cociero	Faulted terrace	Upper unit	T-CO1711	60 ± 2	OSL	15,0 ± 1,0	TL	(Gutiérrez et al., 2008, 2020a; Lafuente, 2011; Lafuente et al., 2014)
							15,6 ± 1,3		
		Colluvium		T-CO1712	7589 - 7486 cal BP	^{14}C	15,0 ± 1,0		
Teruel	**Pitarque**	Valdelobos Stream Terrace		T-PI1713	307 ± 25	ESR	76 ± 5	TL	(Gutiérrez et al., 2020a; Simón et al., 2012, 2017)
							71,8 ± 5,1		
							70,7 ± 5,3		
							48,5 ± 3,8		
							78,3 ± 5,2		
							46,5 ± 3,2		
							50 ± 3,4		
Daroca		Pediment deposits		T-DA1715	329 ± 43	ESR	112,8 ± 9,1	TL	(Gutiérrez et al., 2008, 2020a, 2020b)
							118,7 ± 16,2		
Munébrega W		Pediment deposits		T-CAL1716	241 ± 50		71,8 ± 5,5	TL	(Gutiérrez et al., 2009, 2020a)
							41,1 ± 2,7		
					235 ± 54	ESR	32,6 ± 2,5		
							19 ± 1,2		
							9,9 ± 0,6		

3.1. The UAM luminescence lab protocol

So far, very limited information on the methodology applied by the UAM Luminescence Lab has been published, making difficult assessing the validity of their approach and the reliability of their results (Table SD1 in Supplementary Data).

To our best knowledge, the only research articles in which the methods used by the UAM Luminescence Lab are sufficiently explained, correspond to publications in which they dated ceramics and burnt flint (Barandiarán et al., 2007; Calderón et al., 1988). In these studies, they applied the TL *"fine grain"* dating technique (Zimmerman, 1971), in which no mineral separation is performed. After crushing the sample, the grain size 2–10 μm was selected by differential settling in acetone and the resulting polymineral fraction was deposited in a monolayer on a 1 cm diameter aluminium disc. Then, the additive dose procedure was used to determine the Equivalent Dose (D_E). The increasing doses were supplied by a $Sr–Y^{90}$ source with a dose rate of 0.0404 Gy/s. Since the diameter of the grains (<0.01 mm) is lower than the mean range of the α particles (0.02 mm), the calculation of the dose rate (D) takes into account the α, β and γ radiations. At the UAM Luminescence Lab, the β contribution from K was determined using a Geiger-Müller counting system whereas the α activity from U and Th present in the samples was measured using a solid scintillation counting system (ZnS). The γ radiation and cosmic dose rate values were obtained from a private and unpublished radiation map of the Iberian Peninsula produced by the UAM Luminescence Lab from measurements taken with a NaI(Tl) scintillation counter (Bricon Micro Analyst) (UAM Luminescence Lab, personal communication). Such a procedure is of doubtful reliability since the calculation of the cosmic dose rate depends on latitude, altitude and the overburden thickness (Prescott and Hutton, 1988, 1994), and it is not known whether the UAM Luminescence Lab accounted for these parameters in their calculations. In addition, it is also unknown if the water content of the samples was estimated. The higher the water content, the less radiation is absorbed by the minerals. This parameter is one of the main sources of uncertainty in the final age estimate and needs to be calculated as precisely as possible (Grün, 1994).

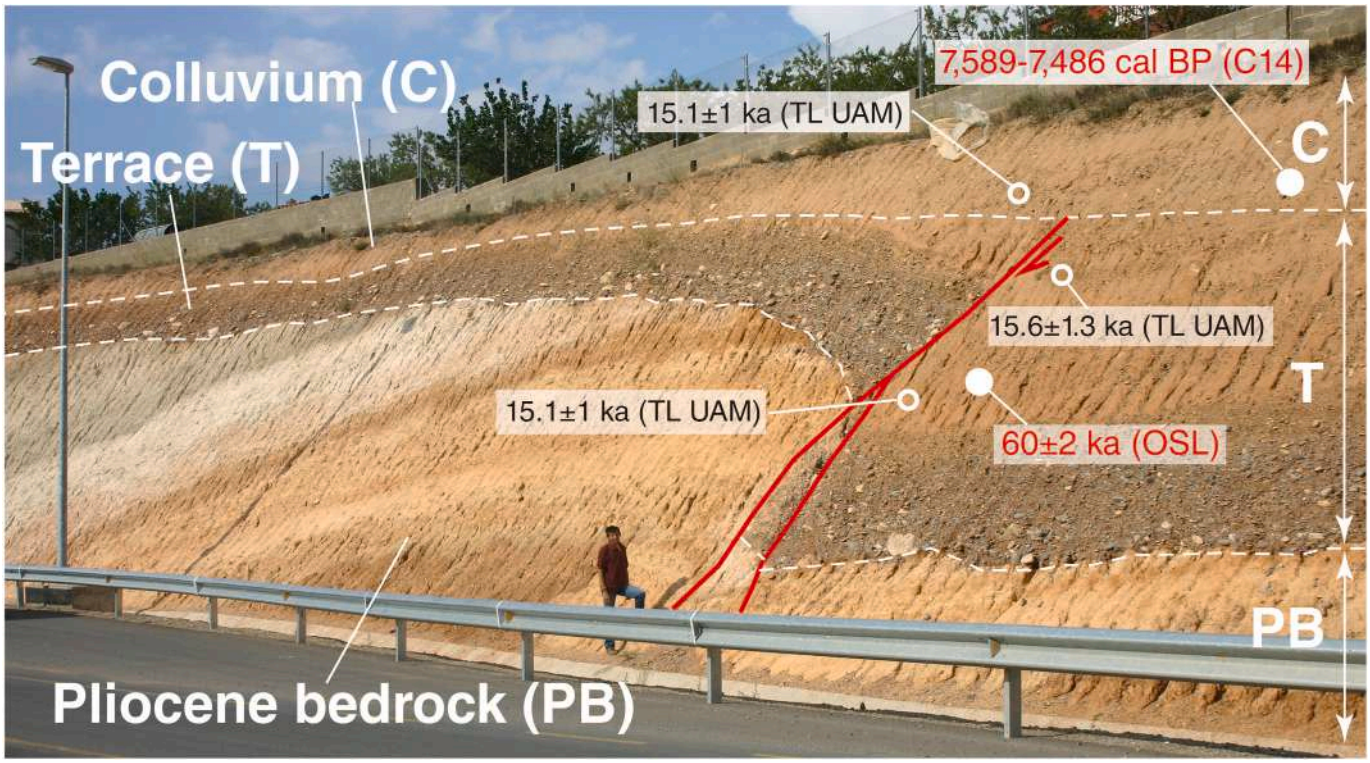

Fig. 3. Image of Cociero site, showing a faulted terrace unconformably overlying Pliocene bedrock, and a non-deformed colluvial deposit that truncates the fault. Previous ages from the UAM Luminescence Lab (TL UAM) with black characters and new ages in red (C14: radiocarbon dating).

Dating naturally occurring sediments is not quite as straightforward as burnt materials. In the case of pottery, the exposure to heat during firing removes any TL signal accumulated in the minerals whereas for sediments, no heating occurs at the time of deposition (Aitken, 1989; Wintle, 2008a; Wintle and Huntley, 1982). This major difference has important repercussions in the protocols to be used for calculating ages. Sediments must have been exposed to sunlight during transportation and bleached prior to burial. The major reason for not using TL dating on sediments is the presence in the TL signal of a component that could not be removed by sunlight exposure (Wintle, 2008a). It has also been reported that the use of ultraviolet TL (UG-11: 300–380 mm) filter causes underestimation of the obtained TL ages (Debenham, 1985; Kusiak and Lanczont, 2000). Furthermore, it is required to isolate quartz and feldspar grains from polymineral sediments. Since 1985, two new methods have been systematically used to date sediments rather than TL, both based on the same luminescence physical basis: Optically Stimulated Luminescence (OSL) (Huntley, 1985) and Electron Spin Resonance dating (ESR) (Yokoyama et al., 1985). However, it appears that the UAM Luminescence Lab continued to use the TL *"fine grain"* method (Zimmerman, 1971) for sediments just as it is used for pottery, thus making the assumption that minerals are *"zeroed"* at the time of sedimentation and ignoring the existence of other luminescence dating methods more suitable to date unburnt materials (Duller, 2004; Grün, 1989).

A comprehensive comparison of the protocols used by the UAM Luminescence Lab and those applied by the OSL and ESR laboratories at the CENIEH is discussed by Gutiérrez et al. (2020a).

4. Methods

4.1. Sampling

Two field campaigns were carried out in July 2017 and January 2018 to collect geochronological samples in multiple sites with exposures of deformed and non-deformed Quaternary deposits associated with active faults. A total of sixteen samples were collected in six outcrops which were analyzed by four different dating methods (Table 2 and Fig. SD1 in Supplementary Data): Electron Spin Resonance (ESR: 7 samples), Optically Stimulated Luminescence (OSL: 3 samples), Uranium–Thorium (U/Th: 3 samples) and radiocarbon (^{14}C: 3 samples) dating. Most of the samples were collected in the same layer or in the same morphostratigraphic unit (e.g., terrace deposit) from which previous TL and U/Th numerical ages were available from the literature.

4.1.1. ESR and OSL dating

A total of seven ESR samples were collected from the following sites (Tables 1 and 2): (1) three samples (PI: T-BAN1701; PII: T-BAN1704 and T-BAN1705) from faulted fluvial-alluvial deposits in the downthrown block of Concud Fault at Los Baños site. See Section 2.1.1.1 and Fig. 2; (2) one sample (T-BAN1708) from a fluvial terrace in the footwall of Concud Fault at Los Baños site. See Section 2.1.1.1 and Fig. 2; (3) one sample (T-PI1713) from a terrace of a tributary of the Turia River (Valdelobos Stream) offset by Teruel Fault (Simón et al, 2012, 2017). See Section 2.1.2.1 and Fig. 5; (4) one sample (T-DA1715) from a pediment deposit displaced by the Daroca Fault (Gutiérrez et al., 2008). See Section 2.2 and Fig. 6; (5) one sample (T-CAL1716) from a pediment deposit offset by the Munébrega W Fault next to a previous paleoseismological trench (Gutiérrez et al., 2009). See Section 2.3 and Fig. 7.

The three OSL samples were collected from the following sites (Tables 1 and 3): (1) one sample (T-BAN1703) from faulted fluvial deposits in the downthrown block of Concud Fault at Los Baños site (Gutiérrez et al., 2008). See Section 2.1.1.1 and Fig. 2; (2) one sample (T-CO1711) from a terrace affected by a secondary fault situated close to the Concud Fault at Cociero site (Gutiérrez et al., 2008; Lafuente, 2011; Lafuente et al., 2011). See Section 2.1.1.2 and Fig. 3; (3) one sample (T-MAT1714) from the deposit of a mantled pediment at Mataueta site, in which a paleoseismological trench was previously excavated to investigate Concud Fault (Ezquerro et al., 2014). See Section 2.1.1.3 and Fig. 4.

Since OSL and ESR sampling conditions are very similar, the ten samples analyzed by these techniques were collected following the

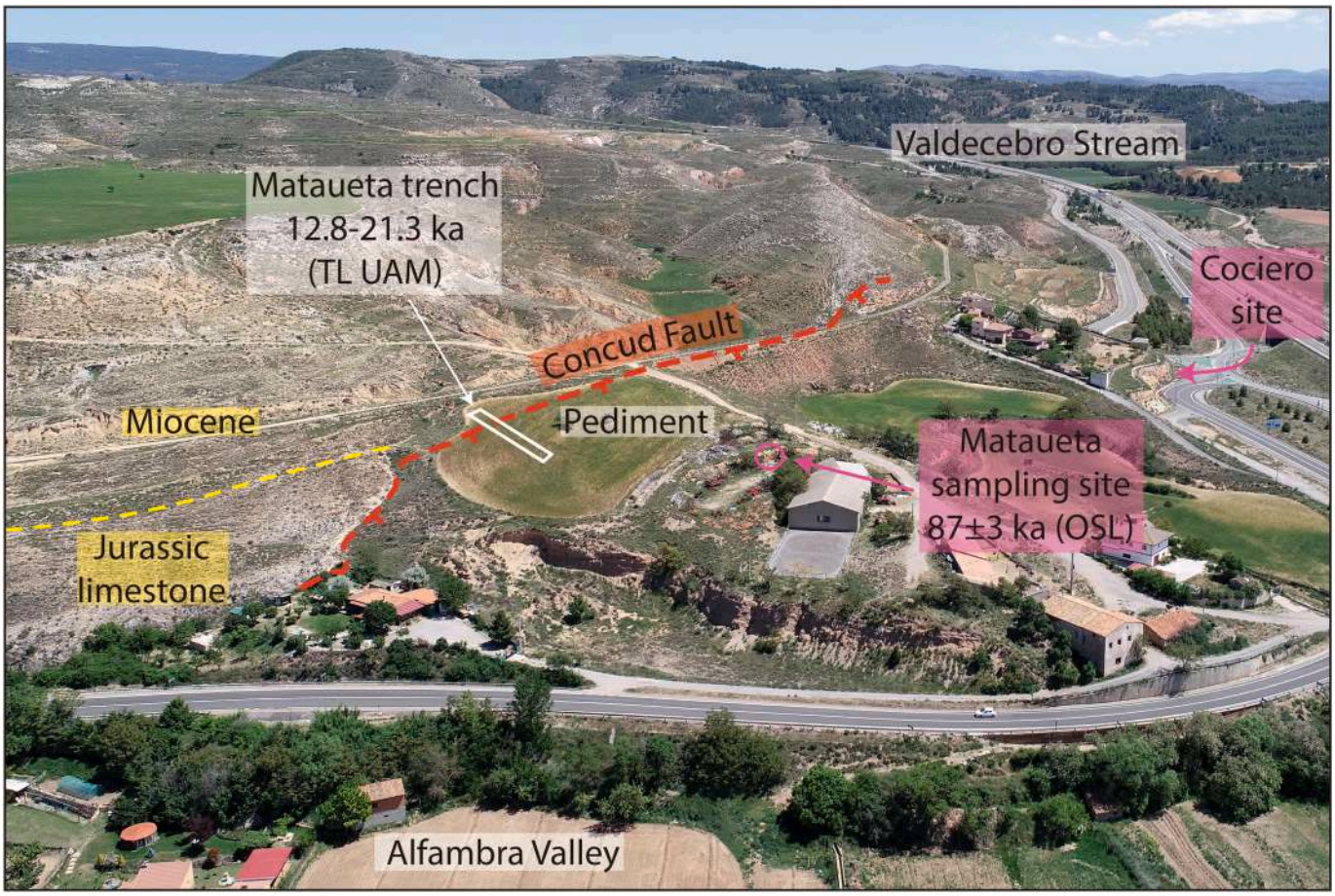

Fig. 4. View of the left margin of the Alfambra River valley showing the location of Matraueta and Cociero sites associated with the southern termination of the Concud Fault segment. The image indicates the location of the trench dug across the Concud Fault in a pediment deposit, which was dated at 12.8–21.3 ka at the UAM Luminescence Lab. A sample collected from the same pediment in a more distal position has yielded and OSL age of 87 ± 3 ka.

methodology described in Moreno et al. (2017) (Fig. SD1 in Supplementary Data). Samples for Equivalent Dose (D_E) analysis were taken using a light-proof container (PVC tube) in most cases. On one occasion, the sediment was too hard to insert the tube and the sample was collected by carving out a block of sediment. On four occasions, neither PVC tube nor block extraction were feasible, hence the sandy matrix within the gravelly deposit was scooped out into a light-proof container under an opaque plastic cover (Table 2). A bulk sediment sub-sample for external dose rate (D) calculation was also collected from each sampling point for high-resolution γ-ray spectrometry (HRGS) analysis. *In situ* gamma spectrometry measurements taken within each sampled hole were obtained inserting either a NaI(Tl) or a $LaBr_3$(Ce) probe, each connected to an Inspector1000 multichannel analyzer (Canberra).

4.1.2. U/Th series dating

Three samples of faulted tufa deposits were collected from two different stratigraphic units situated on both sides of the Concud Fault (Los Baños site), at the west margin of the Alfambra River valley (Tables 1 and 2; Fig. 2 **and SD1 in Supplementary Data)**. A recent active quarry located in the tufa unit capping the Alfambra terrace offers fresh exposures up to 4 m high. Samples were collected in two different facies: phytoherms of macrophytes consisting of stems in life position (sample T-BA-SU-1), and a laminated bioherm of bryophytes (sample T-BA-SU-2). See Section 2.1.1.1 and Fig. 2. The other stratigraphic unit sampled (sample T-BA-SU-3) corresponds to a 0.2–0.5 m thick micritic tufa layer exposed in the downthrown block of Concud Fault (unit I3 of package PI in Fig. 2). The selection of the sampling points was based on the examination of hand specimens for the identification of the most favorable facies, trying to avoid rocks with evidence of secondary porosity and cementation. All samples were collected by mechanical percussion with chisel and hammer. The fragments obtained were placed in individual plastic bags with their corresponding codes.

4.1.3. Radiocarbon dating

A total of three samples were collected for Accelerator Mass Spectrometry (AMS) radiocarbon dating at two sites associated with the Concud Fault (Fig. 2). They were extracted with a knife and plastic bags after careful cleaning of the exposures. The three of them were identified as small black pieces of detrital charcoal. A truck with an articulated boom lift was used for sampling the different units, all of them at high elevation in artificial cuttings.

The two samples from Los Baños site were collected from the two fissure fills exposed in the downthrown block and associated with the fault (See Section 2.1.1.1 and Fig. 2). Sample T-BAN-1706 was extracted from the youngest fissure fill (unit FF3) juxtaposed to the fault plane (Fig. 2). This unit, which represents the youngest faulting event recorded at the site, consists of a massive, cream-colored sandy silt with scattered pebble- and cobble-sized clasts. Sample T-BAN-1707 was retrieved from the intermediate fissure fill (unit FF2 in Fig. 2), flanked by the FF3 unit and colluvial deposits. The deposit of the intermediate fissure consists of massive, light-orange silts with scattered gravel-sized clasts and some large boulders of conglomerate with subvertical fabrics. The two sampled fissure fills display a net contact that can be traced with confidence thanks to the different color of the deposits. The fissure fills can be interpreted as short-transport colluvial facies shed from the fault scarp (footwall) and trapped in ground fissures soon after their opening

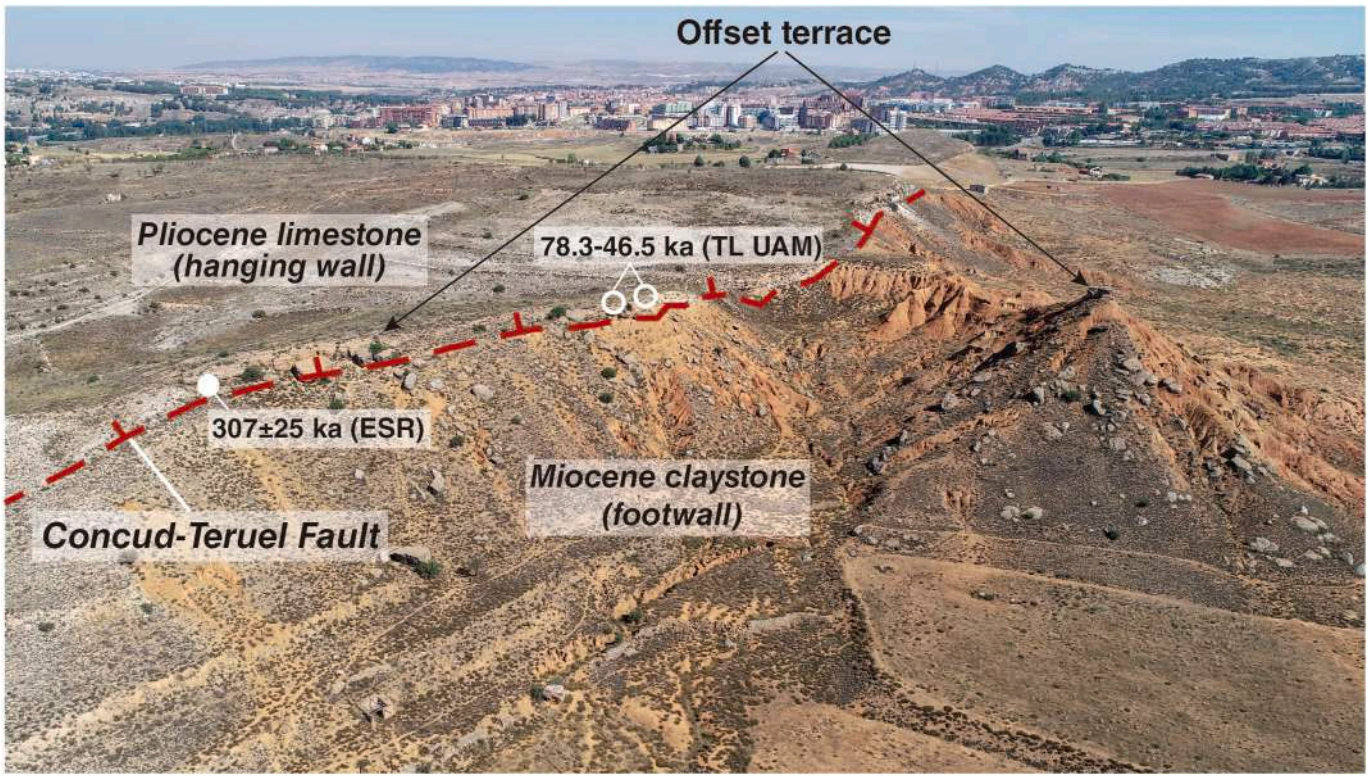

Fig. 5. View of Pitarque site, where the Teruelo segment of the Concud-Teruel Fault juxtaposes Miocene claystome agains Pliocene limestone and ofsets a terrace of the Valdelobos Stream situated 60 m above the thalweg. A new ESR age of 307 ± 25 ka has been obtained from this terrace, whereas the six ages provided by the UAM Luminescence Lab ranged between 78.3 and 46.5 ka. The youngest one was used in previous studies to estimate the slip rate of the fault segment. Teruel city in the background.

by coseismic surface ruptures. These fissure fills were previously TL-dated at the UAM Luminescence Lab (Lafuente et al., 2011) (Fig. 2).

The sample from Cociero site (T-CO-1712) was collected from a non-deformed colluvial deposit that truncates a fault, which offsets a terrace deposits of the Alfambra River (Fig. 3). The sampled colluvial deposit, around 3 m thick, consists of crudely-bedded matrix-rich angular gravels and clayey sands with scattered clasts. The charcoal piece was found in a sandy layer 0.3 m above the basal unconformity of the colluvial deposit. This colluvial deposit was previously dated by TL at the UAM Luminescence Laboratory (Lafuente et al., 2011) (Fig. 3).

4.2. ESR dating of quartz grains

4.2.1. Sample preparation

Sample preparation was carried out at the ESR dating Laboratory of the Centro Nacional de Investigación sobre la Evolución Humana (CENIEH) (Burgos, Spain) in a dark room according to the following protocol: (1) separation of the 100–200 μm grain-size fraction by wet sieving; (2) elimination of carbonates and organic matter from the selected fraction by HCl (32%) and H_2O_2 (30%), respectively; (3) removal of heavy minerals and feldspars by density segregation using sodium polytungstate (SPT) at d = 2.68 g/cm^3 and d = 2.58 g/cm^3; (4) withdrawal of magnetic minerals passing a neodymium magnet over the sediment. Samples were then treated with HF (40%) during 40 min to eliminate the remaining feldspars and to etch quartz grains. A second round of HCl (32%) was applied. Finally, samples were dry sieved in order to isolate the final pure quartz grains within the 100–200 μm grain-size fraction (Table SD1 **in Supplementary Data)**.

The Multiple Aliquots Additive dose (MAAD) approach for dating quartz grains was applied **(**Table SD1 **in Supplementary Data)**. Each sample was divided into 10 multiple grain aliquots. Eight of these aliquots were irradiated using a calibrated Gammacell-1000 ^{137}Cs gamma source (dose rate ~ 8 Gy/min) at the following doses: 150, 300, 600, 1200, 2400, 5000, 10000 and 15000 Gy. For each sample, one aliquot was preserved natural (no irradiated and no bleached) and one aliquot was optically bleached for around 1500 h using a SOL2 (Dr. Hönle) solar light simulator in order to evaluate the ESR intensity of the non-bleachable residual signal associated with the Aluminium center of quartz (Voinchet et al., 2003).

4.2.2. ESR dose reconstruction

The Multiple Center approach (Toyoda et al., 2000) was applied to the ESR samples **(**Table SD1 **in Supplementary Data)**. The method is based on the assumption that all the centers measured in a given quartz sample should provide similar dose estimates. However, due to the different bleaching kinetics of Aluminium (Al) and Titanium (Ti) centers (Tissoux et al., 2007), this assumption is rarely met. Thus, if the Al center provides a significantly higher D_E value, then this is most likely due to incomplete bleaching of this signal. Therefore, the Al age should be considered to provide maximum age estimates. If the Ti age estimate is significantly younger than the corresponding Al age estimate, then the former should be considered as the best estimation for the chronology of the deposit (Duval et al., 2015). In this work, both Al and Ti centers were measured and analyzed.

ESR measurements were performed at low temperature (90 K) using a nitrogen gas flow system connected to an EMXmicro 6/1 Bruker X-band ESR spectrometer coupled to a standard rectangular ER4102ST cavity at the ESR laboratory of the CENIEH. To ensure constant experimental conditions over time, the temperature of the water circulating in the magnet is controlled and stabilized at 18 °C by a water-cooled Thermo Scientific NESLAB thermoflex 3500 chiller and the temperature of the room was kept constant at 20 °C by an air conditioning unit. The following experimental conditions were employed for the Al center: 5 mW microwave power, 1024 points resolution, 100 kHz modulation

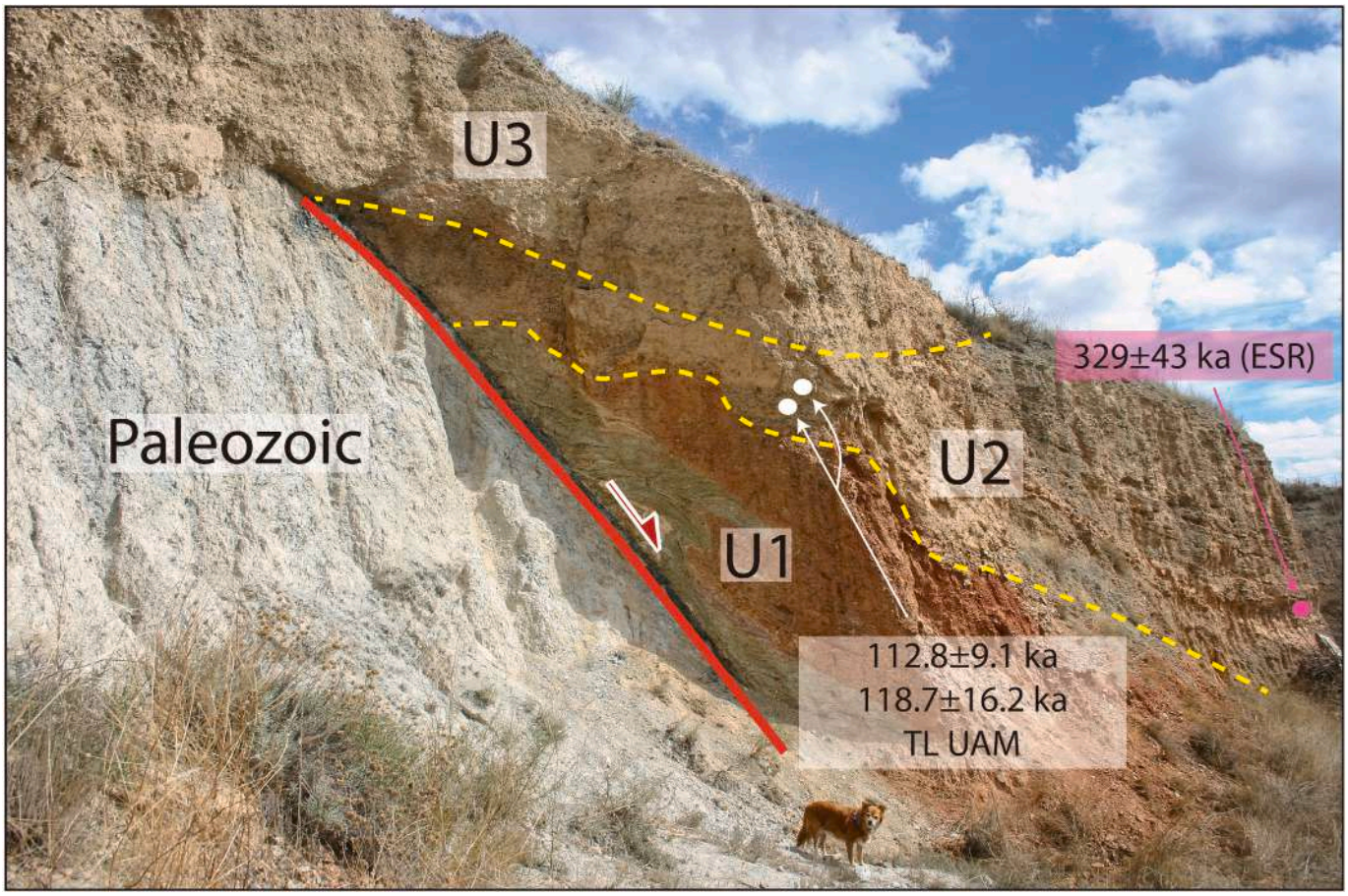

Fig. 6. Image of Daroca Fault site. Here, the Daroca fault juxtaposes Paleozoic bedrock against the red Plio-Quaternary fill of the Daroca Half-graben (U1) and a pediment deposit (U2) inset into the basin fill. The fault is truncated at the site of the image by a recent colluvial deposit (U3). The faulted pediment was dated at ca. 113 and 119 ka by the UAM Luminensce Lab and at 329 ± 43 ka by ESR in this work.

frequency, 1 G modulation amplitude, 40 ms conversion time, 40 ms time constant, 9 mT sweep width and 1 scan. The ESR signal associated with the Ti center was measured as follows: 5 mW microwave power, 1024 points resolution, 100 kHz modulation frequency, 1 G modulation amplitude, 60 ms conversion time, 40 ms time constant, 200 G sweep width and 1–3 scan. The angular dependence of the ESR signal due to sample heterogeneity was taken into account by measuring each of the ten aliquots (one natural, one optically bleached and eight γ-irradiated) three times after a ~120° rotation in the cavity. Furthermore, data reproducibility was checked by running ESR measurements over different days. This procedure was carried out for both the Al and Ti signals.

The ESR intensity of the Al center was extracted from peak-to-peak amplitude measurements between the top of the first peak (g = 2.0185) and the bottom of the 16th peak (g = 1.9928) (Toyoda and Falguères, 2003). The ESR intensity of the Ti centers was measured in three different ways following the recommendation of Duval and Guilarte (2015) **(See** Fig. SD2 **in Supplementary Data)**:

- Peak-to-peak amplitude measurement between g = 1.979 and the bottom of the peak at g = 1.913 (Option A; Ti–Li center)
- Peak-to-baseline amplitude measurement around g = 1.913–1.915 (Option D; Ti–Li center)
- Peak-to-baseline amplitude measurement around g = 1.915 (Option C; Ti–H center).

For each aliquot, ESR intensities of the Al and Ti centers were corrected by the corresponding receiver gain value, number of scans and aliquot mass. Final ESR intensities correspond to the mean value derived from the repeated measurements.

The equivalent dose (D_E) values were calculated with the Microcal Origin 8.5 software using the Levenberg-Marquardt algorithm by chi-square minimization. For the Al center, a single saturating exponential + linear function (SSE + LIN) (Duval et al., 2009) was fitted through the experimental points. For the Ti centers, the Ti-2 function initially proposed by (Woda and Wagner, 2007) was used (Table SD2 **in Supplementary Data)**. With the SSE + LIN function, data were weighted by the inverse of the squared ESR intensity ($1/I^2$), whereas with the Ti-2 function data were weighted by the inverse of the squared error ($1/s^2$), as described in Duval et al. (2015).

4.2.3. *Dose rate and age calculation*

The dose rate is derived from the analysis of radioactive elements in the sample and its surroundings by a combination of *in situ* and laboratory measurements. Around 100 g of raw sediment from each sample were analyzed by high resolution γ-spectrometry (HRGS) in order to derive α, β and γ external dose rate values from U, Th and K contents in powder of raw sediment (Table SD3 **in Supplementary Data)**. External γ dose rates derived from *in situ* measurements were also available thanks to the *in situ* gamma spectrometry performed at the exact sampling spot using NaI(Tl) and $LaBr_3$(Ce) probes connected to an Inspector1000 multichannel analyzer (Canberra) and calculated using the threshold approach (Duval and Arnold, 2013). Total dose rates were calculated using the dose rate conversion factors from Guérin et al. (2011). Values were corrected with β and α attenuations for spherical grains (Brennan, 2003; Brennan et al., 1991) and water attenuation

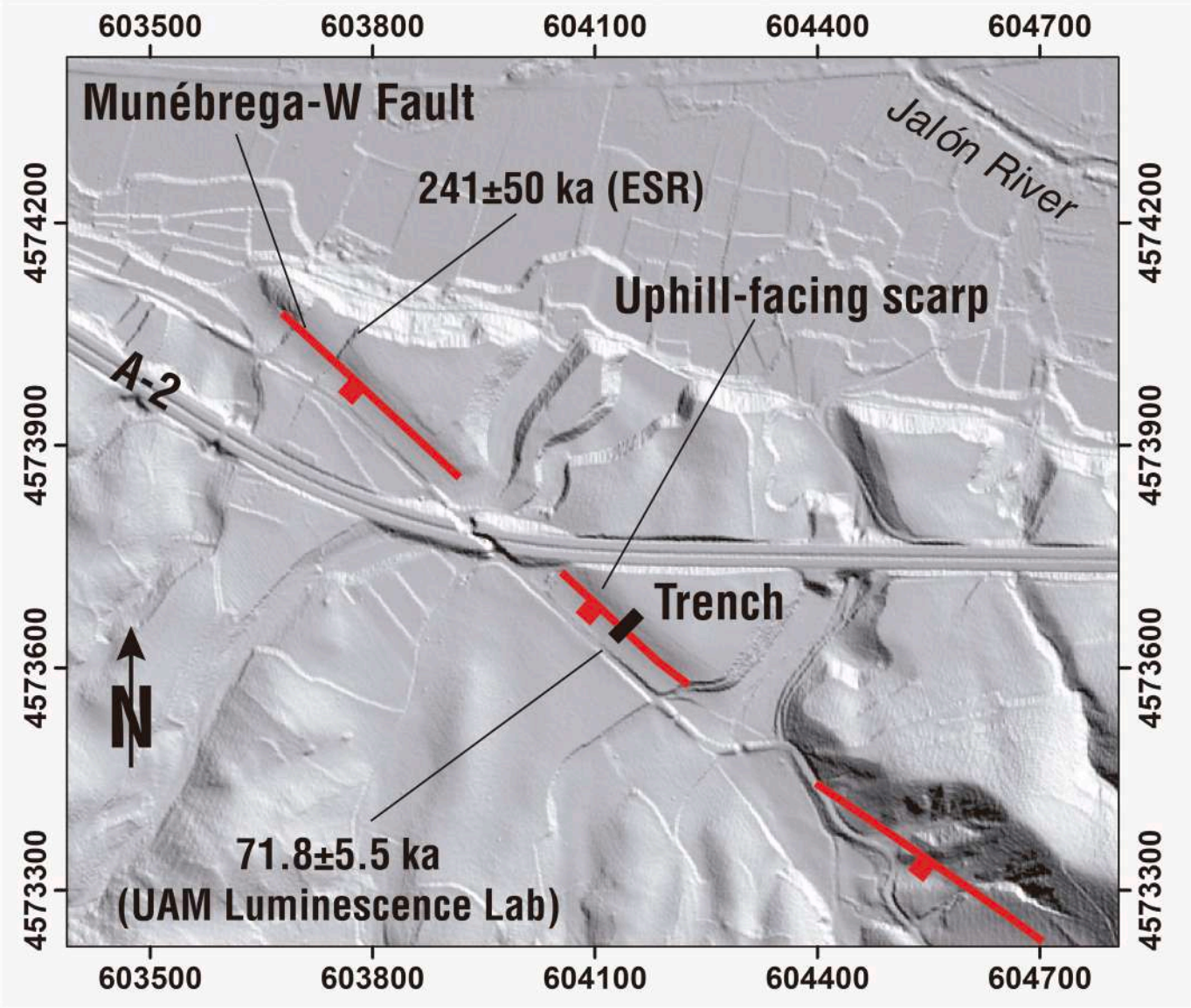

Fig. 7. Shaded relief model of the Munébrega W Fault site, showing the location of a previous trench (Gutiérrez et al., 2009) and the artificial excavation from which a new sample was collected for ESR dating. The image shows a pediment that merges with a terrace of the Jalón River offset by the fault, expressed as an uphill-facing scarp.

formulas from Grün (1994). The final water content used for the dose rate evaluation was assumed to be around 60% of the water content at saturation measured in the laboratory **(**Table SD4 **in Supplementary Data)**. The resulting values range from 14 to 25%. A α-efficiency k-value of 0.15 ± 0.10 (Yokoyama et al., 1985) was assumed for the alpha dose rate. The cosmic dose rate was calculated from the equations of Prescott and Hutton (1994), with latitude, altitude and depth corrections. An internal dose value of 50 ± 30 μGy/a was systematically assumed (Vandenberghe et al., 2008).

ESR age calculation was performed using a non-commercial software based on the open access program Dose Rate and Age Calculator (DRAC) (Durcan et al., 2015) which takes into account the uncertainties derived from concentrations, depth, water content, *in situ* gamma dose rate, attenuations and D_E values. The errors associated with total doses, equivalent doses and ESR age results are given at 1σ (Table 3).

4.3. *Luminescence dating*

4.3.1. *Sample preparation*

Sample preparation was performed at the CENIEH's Luminescence dating Laboratory following standard procedures in a dark room under controlled dimmed light conditions (>2 μW/cm^2; 600–690 nm) to avoid OSL signal depletion before measurements. The sample preparation protocol consists of: (1) wet sieving to separate the target grain size (90–125 μm); (2) chemical treatment with HCl (32%) to remove carbonates and with H_2O_2 (35%) to eliminate organic material; (3) heavy minerals and feldspar were removed by high-density liquid separation (Sodyum Polytungstate, SPT); (4) the quartz extract was subjected to a treatment in concentrated hydrofluoric acid (40%, 40 min) and (5) final dry re-sieving to obtain a better quartz 90–125 μm grain-size fraction. A separate bulk sediment sub-sample was used to carry out water content analysis. This sample was subsequently, ground for beta dosimetry and gamma spectrometry measurements **(See** Table SD1 **in Supplementary Data)**.

Table 2
List of samples collected and sampling techniques used in this work. (BAN: Los Baños site; PI: Pitarque site; DA: Daroca Fault; CAL: Munébrega W Fault; Co: Cociero site; MAT: Mataueta site).

Dating method	Sample	Sampling Method	Geographic Location (UTM)	Altitude a.s.l.	Depth below ground SurfaTo DC: Insert "rowsep" to this entryce (m)	Type of deposit
ESR	T-BAN1701	Drilling	30T 0661519 - 4471437	925	10.8	Grain supported conglomerate overlying fine sand and lutite
	T-BAN1704	Drilling	30T 0661519 - 4471437	927	5.7	Sand and gravel with erosive bases
	T-BAN1705	Hammering PVC tube	30T 0661519 - 4471437	927	2.9	Thick colluvioums made of gravel and pink sand
	T-BAN1708	Drilling	30T 0661537 - 4471565	950	3.5	Fine sediment
	T-PI1713	Hammering PVC tube	30T 0661319 - 4464496	926	2.3	Medium sand unit below cemented conglomerate
	T-DA1715	Drilling	30T 0633778 - 4551333	786	10.5	Fine sand aluvial deposit
	T-CAL1716	Hammering PVC tube	30T 0603776 - 4574058	591	3.3	Sheetflood deposit
OSL	T-BAN1703	Sediment block	30T 0661519 - 4471437	927	8.5	Silt with tufa fragments
	T-CO1711	Hammering PVC tube	30T 0661645 - 4470302	915	2.3	Fluvial sand
	T-MAT1714	Hammering PVC tube	30T 0661666 - 4470526	926	1.4	Fine sand
U- Series	T-BA-SU-1	–	30T 0661738 - 4471802	959	0.53	Quarry
	T-BA-SU-2	–	30T 0661738 - 4471802	959	–	Quarry
	T-BA-SU-3	–	30T 0661519 - 4471437	927	10.5	Fault
Radiocarbon	T-BAN1706	–	30T 661522 - 4471445	935	–	Organic sediment
	T-BAN1707	–		935	–	Organic sediment
	T-CO1712	–	30T 66154 - 4470296	917	–	Organic sediment

Table 3
ESR results obtained on quartz grains for the Concud–Teruel Fault, Daroca Fault and Munébrega W Fault. (Bl: bleaching; D_{int}: internal dose rate; D_{α}: alpha dose rate; D_{β}: beta dose rate; D_{γ}: gamma dose rate; D_{cos}: cosmic dose rate; D: total dose rate; D_E: equivalent dose).

	Concud - Teruel Fault					Daroca Fault	Munébrega Fault
	Los Baños site				Pitarque site		
	PI - Lower package	*PII - Upper package*		*Alfambra terrace*		*Level U2*	*Level A1*
	T-BAN1701	**T-BAN1704**	**T-BAN1705**	**T-BAN1708**	**T-PI1713**	**T-DA1715**	**T-CAL1716**
D_{int} (μGy/a)	50 ± 30	50 ± 30	50 ± 30	50 ± 30	50 ± 30	50 ± 30	50 ± 30
D_{α} (μGy/a)	49 ± 12	33 ± 8	36 ± 8	36 ± 8	33 ± 8	62 ± 15	82 ± 19
D_{β} (μGy/a)	983 ± 18	774 ± 17	819 ± 18	862 ± 20	914 ± 22	1291 ± 26	2283 ± 54
D_{γ} (μGy/a)	466 ± 16	486 ± 17	402 ± 14	601 ± 21	581 ± 21	918 ± 32	1247 ± 43
D_{cos} (μGy/a)	59 ± 6	102 ± 10	155 ± 15	142 ± 14	170 ± 17	35 ± 4	135 ± 14
Bl (%)	51.7 ± 1.3	45.7 ± 1.7	49.0 ± 0.9	58.0 ± 0.6	58.6 ± 0.4	58.3 ± 0.8	56.6 ± 0.1
D (μGy/a)	1607 ± 41	1446 ± 41	1461 ± 42	1691 ± 45	1748 ± 46	2357 ± 53	3797 ± 79
D_E (Gy) Al	1150 ± 136	654 ± 34	686 ± 66	916 ± 94	1048 ± 99	1545 ± 191	2792 ± 298
D_E (Gy) Ti–Li D option	771 ± 68	538 ± 39	289 ± 22	551 ± 50	537 ± 42	1428 ± 265	915 ± 187
D_E (Gy) Ti–H C option	569 ± 63	438 ± 51	185 ± 24	385 ± 33	424 ± 33	776 ± 100	894 ± 206
Age (ka) Al	716 ± 87	452 ± 27	469 ± 47	542 ± 57	599 ± 59	655 ± 82	735 ± 80
Age (ka) Ti–Li D option	**480 ± 44**	**372 ± 29**	**198 ± 16**	**327 ± 31**	**307 ± 25**	606 ± 113	**241 ± 50**
Age (ka) Ti–H C option	354 ± 40	303 ± 36	127 ± 17	228 ± 20	242 ± 20	**329 ± 43**	235 ± 54

4.3.2. OSL dose evaluation

OSL dose evaluations were carried out using a Single Aliquot Regenerative-dose protocol (SAR) (Murray and Wintle, 2000). Details of measurement protocols are presented in Supplementary Data (Table SD5). Every sample was mounted on stainless steel discs using a 2 mm silicone-sprayed mask. Quartz OSL measurements were carried out using automated Risø TL/OSL DA-20 luminescence readers of the CENIEH equipped with $^{90}Sr/^{90}Y$ beta sources with dose rates around 0.10 Gy/s. Luminescence was detected using bialkali EMI 9235QB15 photomultiplier tubes trough a 7.5 mm Hoya U-340 filter. Stimulation used blue light (470 ± 30 nm). Preliminary tests prior to the final Equivalent Dose (D_E) measurements **(**Fig. SD3 **in Supplementary Data)** included preheat-plateau, thermal transfer, dose recovery and Infra-Red depletion assessments. A preheat-plateau test with increasing temperatures between 180 and 280 °C (held for 10 s) and a cut heat 20 °C below the preheat temperature was performed for all samples. Results are shown in Supplementary Data (Fig. SD4). A dose recovery test was conducted on quartz from sample T-BAN-1703. The test consisted of a double bleach for 500 s at 30 °C, with a 1500 s pause between stimulations. Then, aliquots were irradiated with a known beta dose, equal to the estimated D_E. Resulting ratios average 0.95 ± 0.04. Acceptance criteria applied to all measured aliquots combined several paramaters: IR depletion ratio (<10% (Duller, 2003),), natural normalized signal (L_x/T_x) above saturation of the dose response curve (De < 2*D0), recycling ratio <10%, recuperation <10% and sensitivity change <10%.

In the event of OSL signal saturation occurring in any of the samples during the initially applied tests, prior to the final D_E measurement using

the conventional OSL approach, thermally-transferred – OSL (TT-OSL) was the chosen measurement method to obtain the final D_E distribution of the saturated sample. To date, multiple authors have demonstrated the efficiency of recovering reliable OSL ages applying the TT-OSL approach (Adamiec et al., 2010; Chapot et al., 2016; Hernandez et al., 2012; Porat et al., 2009). TT-OSL signals originated from deeper traps with higher saturation levels can also produce reliable natural fast component signals. Some of those studies have shown that OSL test dose corrections may produce inaccurate TT-OSL dose-recovery results whereas TT-OSL test dose corrections (Stevens et al., 2009) can produce reliable TT-OSL dose recovery results (Arnold and Demuro, 2015). In order to ensure the reliability of our TT-OSL measurements, a dose-recovery test was performed on the sample in question (See Section 5.2) in order to acknowledge the suitability and reliability (i.e., lack of thermal transfer) of the TT-OSL approach.

The final accepted D_E values were estimated using Analyst 4.31.9 (Duller, 2015). An interpolation of the natural sensitivity-corrected signal (L_x/T_x) onto the dose response curve fitted using a single saturating exponential function with 7–9 regenerative doses was used. Final D_E values were estimated following the Central Age Model (CAM) if overdispersion (OD) values were <20% and following the Minimum Age Model (MAM) when OD > 20% (Duller, 2008; Galbraith and Roberts, 2012). When applying the MAM, a 3-parameters Minimum age Model was used to estimate the paleodose, and a sigmab value of 0.2 was assumed.

4.3.3. Dose rate evaluation and age calculation

Total dose rate values were derived from a combination of *in situ* and laboratory measurements, which included (1) water contents and maximum water saturation in the laboratory, (2) *in situ* gamma spectrometry with a portable gamma spectrometer (Canberra InSpector 1000 coupled with a 1.5*1.5 inch NaI (Tl) probe) and calculated using the Threshold approach (Duval and Arnold, 2013), (3) beta spectrometry with a (RISØ) low-level beta multicounter, and (4) elemental concentration determination of ^{238}U, ^{232}Th and ^{4}K by high resolution gamma spectrometry (HPGS) with Hyperpure Germanium (HPGe) detector. For dosimetry calculation, conversion factors from Guérin et al. (2011) have been used. Grain size attenuation factors (Brennan, 2003; Brennan et al., 1991; Guérin et al., 2011), water content (Aitken and Xie, 1990) and etching attenuation factors (Brennan, 2003) were applied. Cosmic dose rate was calculated following Prescott and Hutton (1994). Total dose rate and ages were calculated using DRAC v1.2 (Dose Rate and Age Calculator, Durcan et al., 2015) Age estimations are given at 1σ (Table 4).

Table 4
Summary of OSL results on quartz grains, including dosimetry calculations, D_E values and final ages. (Ḋ: Dose Rate; N: number of aliquots that passed SAR acceptance criteria/total measured aliquots; OD = Overdispersion; D_E: Equivalent Dose. CAM: Central Age Model. MAM: Minimum Age Model).

		Los Baños site	Cociero site	Mataueta site
		T-BAN-1703	T-CO-1711	T-MAT-1714
Dosimetry	Water content (%)	18.52 ± 0.25	19.27 ± 0.30	15.63 ± 0.24
	$\dot{D}_\beta$ (μGy/a)	784 ± 31	1165 ± 44	876 ± 34
	$\dot{D}_\gamma$ (μGy/a)	418 ± 15	403 ± 15	418 ± 15
	$\dot{D}_{cosmic}$ (μGy/a)	81 ± 20	159 ± 20	177 ± 20
	Total Ḋ (μGy/a)	990 ± 33	1320 ± 40	1180 ± 40
	^{238}U concentration (ppm)	2.22 ± 0.03	2.13 ± 0.03	2.28 ± 0.03
	^{232}Th concentration (ppm)	3.99 ± 0.10	6.38 ± 0.19	4.01 ± 0.13
	^{40}K concentration (%)	0.64 ± 0.02	1.17 ± 0.03	0.80 ± 0.02
D_E	Grain size fraction (μm)	90–125	90–125	90–125
	Method	TT-OSL	OSL	OSL
	Protocol	SAR	SAR	SAR
	No. Regenerative Doses	9	9	7
	Pre-Heat (°C)	220	200	260
	N	14/36	23/24	23/24
	OD (%)	42	14.4	6.9
	Age Model	MAM	CAM	CAM
	D_E CAM (Gy)	699.2 ± 61.4	79.2 ± 2.3	102.8 ± 1.7
	D_E MAM (Gy)	274 ± 33	–	–
Age	MAM Age (ka)	**276.86 ± 34.59**		
	CAM Age (ka)	**706.30 ± 69.53**	**59.98 ± 2.49**	**87.08 ± 2.97**

4.4. U/Th series dating

4.4.1. Sample preparation

Sample preparation was conducted at the Uranium series Dating Laboratory at CENIEH. Bulk samples were cut using a diamond layered saw and precleaned using diluted HCl rinsed with deionized water. Subsequently, samples were dried in clean conditions. Samples T-BA-SU-1 and T-BA-SU-2 were also polished carefully in order to remove spurious material and reveal possible internal structure such as layering or lamination. Sample T-BA-SU-3 was too friable to produce polished surfaces.

As it is well known, Uranium and Thorium (U/Th) dating of calcareous tufa is problematic due to the frequent presence of detrital and/or organic material (Garnett et al., 2004). Therefore, before chemical separation and purification, the samples were inspected for detrital particles and cleaned by sonication (10 min) in MilliQ water to wash out the pores of the calcareous material. Subsamples (50–150 mg) of the tufa specimens were extracted using a micro-drill with a tungsten carbide tip (1 mm diameter). The most compact parts of the tufa samples with primary texture were selected for the extraction of the subsamples in order to avoid pores, root traces, solution features and secondary cements.

Ultrapure water (R > 18.2MΩ cm) was obtained from a MilliQ A10 water purification system (Millipore) starting from previously purified water from an Elix purification system (Millipore). Trace metal grade 14M HNO_3 and 12M HCl were further sub-boiling bidistilled (Savillex DST-1000) in order to keep the reagent background as low as possible. 30–32% (v/v) H_2O_2 and 1M H_2O_2 solutions were prepared by the convenient dilution from the ultra-purity grade (UPa) products acquired from ROMIL™.

Samples were dissolved, spiked with an addition of a gravimetric dilution of IRMM 3636a standard for ^{236}U and NIST SRM 4328c for ^{229}Th, so that the intensities at the detectors were as close to the analytes as possible, and homogenized in 7M HNO_3. The digestion was carried out by using a sequence of HNO_3 – H_2O_2 – HCl. After drying the residue and reconstituting it into 6M HCl, U and Th were separated in a strong acid anion AG 1X-8 resin using the gravity-column method. Each fraction was then purified using UTEVA anion resin columns. Finally, purified U and Th solutions were put in 0.36M HCl for the measurement procedure.

4.4.2. MC ICP-MS measurements

U and Th concentrations and isotopic ratios measurements were carried out with a Multicollector Inductively Coupled Plasma Mass Spectrometer (MC ICP-MS, Thermo Scientific Neptune). The samples were introduced into the plasma using a 50 μl min^{-1} PFA concentric nebulized assembled on a Scott type PFA spray chamber carrying the sample into an Aridus II membrane desolvator (Cetac). Isotope ratios $^{234}U/^{238}U$, $^{235}U/^{238}U$, $^{236}U/^{238}U$, $^{229}Th/^{232}Th$ and $^{230}Th/^{232}Th$ were measured in low-resolution mode, with the Faraday collectors connected to $10^{11}\Omega$ resistors and the central SEM. Instrument settings and data acquisition parameters are summarized in Table SD6. Two

independent measurement sequences for U and Th were run after applying the sample introduction settings and instrumental fine tuning. Acid blank (0.6M HCl) and procedural blank were checked several times along the measurement sequence to evaluate their contribution to the analyte signal intensity.

The isotope ratios were measured by the standard bracketing method with errors below 5%. Mass bias was checked by measurements of the standard solutions IRMM 183, IRMM 184 (uranium) and IRMM 35 and IRMM 036 (thorium) and the exponential law was followed. The concentrations of ^{238}U and ^{232}Th were calculated by the isotopic dilution mass spectrometry (IDMS) method.

4.5. Radiocarbon dating

Radiocarbon samples were analyzed at Beta Analytic Inc. (Miami, Florida) applying the standard AMS isotope counting method of the laboratory. The AMS method measures directly the amount of the unstable ^{14}C isotope in the sample, whereas the less sensitive decay counting method measures the decay rate, requiring larger samples and longer counting times. The following procedures were applied to obtain the ages estimates:

(1) Sample pre-treatment: samples were dispersed, floated and then sieved to <180 μm to remove any rootlet or other macrofossil material. After sieving the sample to <180 μm, no charred fragments larger than that size were found. This is attributed to fragmentation of the original charcoal samples during transportation in a non-rigid container (i.e., plastic bags). Therefore, the samples were treated as organic sediment and dated on the bulk-organic fraction. Subsequently, they were treated serially with HCl acid at 70–90 °C to remove any carbonates. Then, the sediments were rinsed to neutral with deionized water and dried at 90 °C. They were then homogenized and a small aliquot was separated and tested with concentrated HCl to verify that carbonate species were completely removed.
(2) CO_2 generation and measurement of the $\delta^{13}C$: The sediment was then combusted by an active oxygen stream within an enclosed vacuum system. The CO_2 derived from the combustion was dried and cryogenically purified to remove water vapor and any non-combustible/condensable gases using a series of dry-ice/methanol water traps at ca. −78 °C. A small amount of the CO_2 generated during the combustion was used to measure the $^{13}C/^{12}C$ ratio with an ordinary thermo Delta-Plus isotope ratio mass spectrometer. This ratio, expressed as $\delta\ ^{13}C$, is used in the calculation of the conventional radiocarbon age to correct for isotopic fractionation, which is unrelated to time.
(3) Conversion of CO_2 to graphite: the purified and dry CO_2 was then converted to graphite in a graphitization cell under vacuum to produce the elemental carbon for measurement by AMS. The CO_2-graphite conversion was achieved through the Bosch reaction, in which carbon dioxide and hydrogen sequentially react at 550–650 °C with the aid of a cobalt powder catalyst (free of any carbon contaminants) to produce elemental carbon (graphite), water and heat. Water generated in the graphitization processes is continuously removed via a cold finger by a dry-ice Methanol slush. Once graphitization has gone to completion (yield >80%), the graphitization cell is placed under a vacuum and allowed to warm to room temperature drying the graphite. The graphite is then purged 1x with ultra-pure (99.999) argon to remove any CO_2 and with a silicone drying agent to remove any remaining water vapor.
(4) Cathode preparation and AMS counting: the graphite is placed into an AMS cathode and then compressed to a minimum of 150 psi. The cathode is then placed into a cathode wheel and into the AMS. Radiocarbon AMS counting was performed with a 250Kev NEC single stage accelerator mass spectrometer (NEC SSAMS). The carbon atoms of the sample are converted into charged atoms by bombarding the sample with cesium ions and then focused into a fast-moving beam.
(5) Age estimation and calibration: conventional radiocarbon age, corrected for total fractionation effects, are obtained using the parameters outlined by Stuiver and Polach (1977). These ages were calibrated using the high probability density range method (BetaCal3.21) and the database Intcal13 (Reimer et al., 2013). Conventional radiocarbon ages and sigmas are rounded to the nearest 10 years. For sigmas lower than ± 30 years, a conservative ± 30 BP is cited in the result.

5. Results

5.1. ESR dating on quartz grains

The ESR analytical data and all the ESR Dose Response Curves (DRC) derived from the evaluation of the Al, Ti–Li and Ti–H centers are provided in Fig. 8 and in Supplementary Data **(**Tables SD7**, SD8 and Appendix)**.

5.1.1. Fitting results

Regarding the Al center, all samples show ESR intensity values with a very good reproducibility. The difference between the ESR intensities measured in three different days is less than 4%. Dose equivalent (D_E) values were calculated by considering the ESR intensity measured each day instead of averaging the mean ESR intensities obtained over repeated measurements. The fitting results derived from the Al center (Table SD7) show an excellent goodness-of-fit for all samples (adjusted $R^2 > 0.99$), resulting in relative D_E errors ranging from 5% to 12%. The high reproducibility of the measurements, combined with the good adjustment to the experimental points, indicate the high reliability of the results obtained with the Al center. ESR intensities of the bleached aliquots are within a relatively narrow range between 46% and 57%, suggesting similar bleaching conditions for all samples. These values are close to those obtained from Cuesta de la Bajada site (54–56%) located in a terrace of the Alfambra River valley, very close to the sites of the Concud-Teruel Fault analyzed in this work (Duval et al., 2017a).

Concerning the Ti center, all samples also show ESR intensity values with a very good reproducibility (<5%). The dose equivalent (D_E) values were calculated, as for the Al center, by considering for each aliquot the ESR intensity measured each day. The only exception is T-DA1715 sample which reaches 8%. This worse reproducibility induced a much poorer adjustment of the function using all the measurements. For this reason, in this only case the D_E value was calculated by averaging the mean ESR intensities obtained over 3–5 days. To confirm their reliability, the adjusted R^2 value and the relative errors on the fitted parameters obtained when calculating the D_E from the Ti center, should be greater than 0.98 and lower than 50%, respectively (Duval and Guilarte, 2015). In our samples, the Ti–Li center *(options A and D)* shows adjusted R^2 values higher than 0.98 indicating a high goodness-of-fit and errors ranging between 7% and 18%, with the exception of sample T-CAL1716 (*options A and D*: $R^2 < 0.95$ and errors >25%). It can be observed that *option A* leads to significantly higher D_E values than those obtained with *option D* (Table SD7). This could be due to the influence of the peak at $g = 1.979$ which, taken alone, provides much higher D_E values (Duval and Guilarte, 2015). This pattern has also been observed in regions close to our study area such as Cuesta de la Bajada site (Duval et al., 2017a) and in other fluvial systems such as the Cher River (Middle Loire catchement, France) (Duval et al., 2020). The Ti–H center *(option C)* has also been measured, but the reliability of the fitting results obtained are questionable given the poor goodness-of-fit observed (R^2 ranging between 0.86 and 0.97). Only three samples (T-BAN1708, T-PI1713 and T-DA1715) show adjusted R^2 values greater than 0.98 and relative errors ranging between 8% and 23%.

Our fitting results are consistent with previous observations (Duval

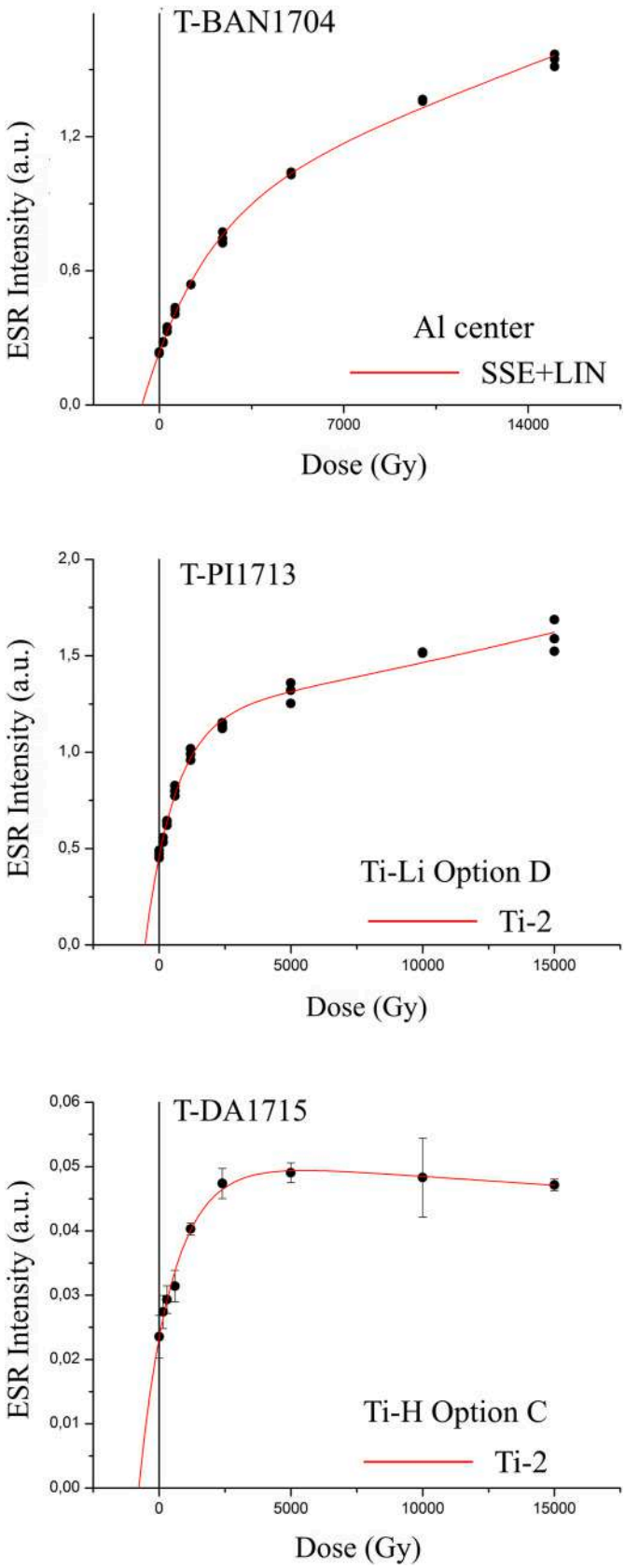

Fig. 8. Examples of three Dose Response Curves (DRC) obtained in this work. All the ESR DRC's derived from the evaluation of the Al, Ti–Li and Ti–H centers are provided in Supplementary Data (SD).

and Guilarte, 2015) and studies (Bartz et al., 2018; Duval et al, 2017a, 2020; Méndez-Quintas et al., 2018; Moreno et al., 2019) that have shown that the more rapidly bleached Ti–Li *(option D)* center provides the most reliable burial age estimates for the deposits (Duval et al., 2017a) (Table 3). Consequently, the final ESR ages for samples collected at Los Baños site (PI: T-BAN1701 and PII: T-BAN1704, T-BAN1705) and Munébrega fault (T-CAL1716) were derived from Ti–Li *(option D)*. However, we have also observed that samples from the Alfambra terrace (T-BAN1708), Pitarque site (T-PI1713) and Daroca Fault (T-DA1715) yielded good fitting results from Ti–H *(option C)*. Consequently, we have considered the D_E values from Ti–H *(option C)* and Ti–Li *(option D)* for age calculations (Table SD7).

5.1.2. Dose rate evaluation

As expected, the gamma dose rates derived from laboratory measurements are between 2% and 15% higher than those obtained from *in situ* measurements (Table SD7). Such a difference is very likely due to the heterogeneity of the sedimentary environment in the vicinity of the samples.

Total dose rate values (D) (Table 3) in the sites of the Concud-Teruel Fault differ slightly to those of Daroca and Munébrega faults. Samples from the Concud-Teruel Fault show the lowest values between 1607 and 1748 μGy/a. In comparison, samples from the Daroca and Munébrega faults have values of 2357 and 3797 μGy/a, respectively. This difference can be attributed to the fact that the Daroca and Munébrega half-grabens are associated with siliceous Cambrian rocks (Gutiérrez et al., 2020a) that contain minerals with higher levels of U, Th and K. However, the outcrops around the Concud-Teruel Fault are dominated by Neogene sediments (mudstones, limestones) and secondarily Jurassic carbonate rocks.

5.1.3. ESR age estimates

The Al center systematically provides the oldest ages whilst Ti–H *(option C)* center yields the youngest, being between 49 and 269% lower than those of the Al center. The differences between Al center and Ti–Li *(option D)* are remarkable, but less pronounced than with Ti–H, ranging from 8% to 205% (Table 3). These results suggest an incomplete bleaching of the Al center due to its slower bleaching kinetics compared to that of the Ti center (Tissoux et al., 2007). Therefore, in accordance with the Multiple Center (MC) approach (Toyoda et al., 2000), the ages obtained from the Al center should be interpreted as maximum age estimates for these deposits.

At Los Baños site, the Ti–Li *(option D)* center ESR yielded an age of 480 ± 44 ka for unit I1 (Lower package) and ages of 372 ± 29 ka and 198 ± 16 ka for two beds that have been sampled in unit PII (Upper package) in the downthrown block. In the footwall, the sample T-BAN1708 yielded a Ti–Li *(option D)* age of 327 ± 31 ka and a Ti–H *(option C)* of 228 ± 20 ka (Table 3). From a methodological point of view, both ages are consistent but geomorphologically, we consider that the Ti–Li *(option D)* center provides a more accurate estimate of the burial age of this deposit. Sample T-BAN1708 has been collected 4.6 m above the base of the terrace deposit with an upper tufa unit up to 7 m thick. This tufa unit has been dated by Gutiérrez et al. (2008) (250 + 32/-25 ka and 213 + 33/-26 ka) and Gutiérrez et al. (2020b) (285.2 ± 14 ka and 228.4 ± 11.4 ka) using U/Th series which is coherent with our age of 327 ± 31 ka for the lower detrital unit of this deposit. These results also suggest that the ages initially proposed by Arlegui et al. (2006) (169 ± 10 ka and 116 ± 4 ka) are minimum values with a large deviation from the actual ones (Fig. 2 and Table 1).

At Pitarque site (+60 m terrace), the sample T-PI1713 yielded a Ti–Li *(option D)* age of 307 ± 25 ka and a Ti–H *(option C)* of 242 ± 20 ka (Table 3). As with sample T-BAN1708, both ages are consistent from a methodological point of view. Nevertheless, the Ti–Li *(option D)* yielded an age closer to those suggested for Cuesta de la Bajada archeo-paleontological site (+55 m terrace) (Duval et al., 2017a; Lisiecki and Raymo, 2005; Santonja et al., 2014) and at Los Baños site (+60–66 m

terrace) (T-BAN1708, this work), both located in nearby terrace deposits of the Alfambra River. The ESR age obtained in the terrace of the Valdelobos Stream faulted by the Teruel Fault (307 ± 25 ka) is also much older than the wide range of numerical ages provided by the UAM Luminescence Lab for the same terrace deposit (78.3–46.5 ka; Simón et al., 2017, 2012). The latter ages are very difficult to justify considering that this terrace is perched 60 m above the thalweg, indicating extremely high incision rates.

In the case of Daroca Fault, the age obtained from Ti–H *(option C)* has been considered the best estimate (Fig. 6 and Table 3). Sample T-DA1715 yielded a Ti–H age of 329 ± 43 ka and close Al and Ti–Li results around 600 ka, all ESR ages are much older than the two OSL ages provided by the UAM Luminescence Lab (113 and 119 ka; Table 1) (Gutiérrez et al., 2008). The ESR age from the pediment faulted by the Munébrega W Fault (241 ± 50 ka) is also much older than that provided by the UAM Luminescence Lab for the same pediment (72 ka; Table 1) (Gutiérrez et al., 2009).

5.2. Luminescence dating

5.2.1. OSL performance

A dose recovery preheat-plateau test was performed on the three OSL samples. Most appropriate preheat temperatures are specified in Table 4. Feldspar contamination was tested using IR stimulation and no detectable signal was observed. To evaluate the different components of the OSL signal, "linearly modulated" OSL (LM-OSL) was performed on all the samples. The OSL signal was dominated by the fast component on all accounts. The number of aliquots passing the rejection criteria varied between 55% and 95% (Table 4 and Fig. 9). Samples T-CO-1711 and T-MAT 1714 show low overdispersion (OD) values of 14.4% and 6.9%, respectively, both under the 20% threshold. Hence, these samples yielded CAM D_E values of 79.2 ± 2.25 Gy and 102.8 ± 1.7 Gy, respectively (Table 4).

For sample T-BAN-1703, 100% of the aliquots measured by conventional OSL SAR protocol (Table SD4) were close to or above saturation (D_0). D_E values obtained for these aliquots are beyond the saturation limit suggested by (Wintle, 2008b) for reliable application of the OSL SAR protocol. Hence, TT-OSL was the method chosen for this sample. TT-OSL measures a luminescence signal (Adamiec et al., 2010; Chapot et al., 2016; Hernandez et al., 2012) in quartz that saturates at much higher radiation doses (up to 4000 Gy) than the traditional OSL signal (Porat et al., 2009). The Stevens et al. (2009) TT-OSL protocol (Table SD5) was used to measure T-BAN-1703, resulting in a high dispersion of the obtained D_E values distribution (OD = 42%), suggesting incomplete bleaching of the sediment. Due to slower kinetics of the TT-OSL signal, the sample may not have been adequately reset during transport and/or deposition. Due to the heterogeneity and multi-modal (multiple D_E population peaks) behaviour of the D_E distribution, CAM should not be used to calculate the age of this sample. Quartz grains with lower paleodoses may be the most suitable ones to calculate the true age of the last burial as they may be better bleached. Thus, MAM was the selected model to calculate the age of sample T-BAN-1703, yielding a D_E of 274 ± 33 Gy. Nevertheless, the proportion of aliquots when applying the MAM with an assumed sigmab value of 0.2 is only 10%. The final number of aliquots used for De calculation may not be enough. Furthermore, it is difficult to discern at a multi-grain level if the MAM isolates aliquots with low TT-OSL lifetimes rather than well-bleached aliquots. We assumed that all aliquots were affected equally by thermal instability, but this D_E value should be handled with caution.

5.2.2. Dose rate evaluation

Laboratory and *in situ* γ spectrometry, together with β dose values and cosmic dose rate provided environmental dose rate values ranging between 990 and 1320 μGy/a (Table 4). Due to the heterogeneity of the sampled units, total environmental dose rates derived from laboratory HRGS are 13–20% higher than the *in situ* gamma spectrometry results.

5.2.3. OSL age estimates

Final OSL age estimates were calculated using the OSL-derived D_E values and environmental dose rates values based on *in situ* and laboratory measurements.

Samples T-CO-1711 and T-MAT-1714 yielded ages of 59.98 ± 2.49 ka and 87.08 ± 2.97 ka, respectively (Table 4). They differ significantly from the ages previously published (Ezquerro et al., 2014; Gutiérrez et al., 2008; Lafuente, 2011; Lafuente et al., 2011; Simón et al., 2016). The ages provided by the UAM Luminescence Lab are around 15 ka for the unit correspond to sample T-CO-1711 and 12.8–27.6 ka for the pediment deposits dated with sample T-MAT-1714. Sample T-BAN-1703 instead, present an OD value of 42% (very large dispersion of 1700 Gy). Hence, D_E value for the final age estimation was calculated using the Minimum Age Model (Galbraith and Roberts, 2012). This sample provides an age of 276.86 ± 34.59 ka. Despite using the MAM, this age exceeds notoriously the 71.7 ± 5.2 ka from previous studies (Gutiérrez et al., 2020b). Dose distributions of the three samples are shown in Fig. 9.

5.3. U/th series dating

The chronology of the three samples collected at Los Baños site was

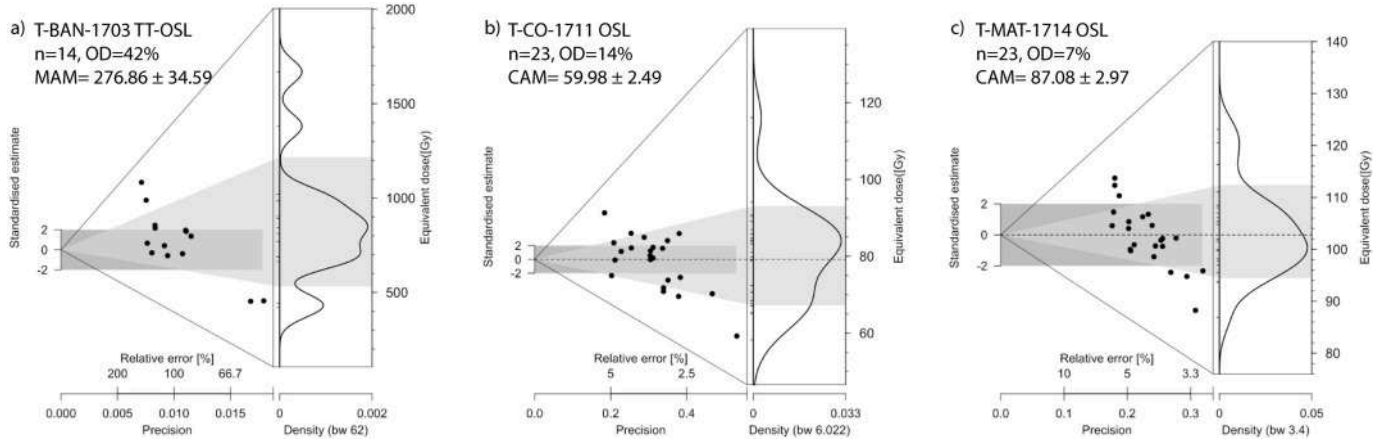

Fig. 9. Luminescence dating results. Multiple-grain equivalent dose (D_E) distributions of samples (a) T-BAN-1703 (TT-OSL), (b) T-CO-1711 (OSL) and (c) T-MAT-1714 (OSL), displayed as abanico plots (Dietze et al., 2016). N = number of aliquots passing rejection criteria. OD = Overdispersion. MAM = Minimum age model. CAM = Central Age Model.

derived from the U/Th disequilibrium method. For this purpose, age estimation has been calculated using the general equation of radioactive decay and the most recent update of radionuclide half-lives (Cheng et al., 2013; Ivanovich and Harmon, 1992). Provided that age corrections for detrital contamination are considered mandatory in those samples with $^{230}Th/^{232}Th$ ratios <20 (Martínez-Aguirre et al., 2019; Toker, 2017), only slight age corrections were expected for our samples. Detrital correction was conducted applying the average crustal $^{230}Th/^{232}Th$ atomic ratio of $4.4 \pm 2.2 \times 10^{-6}$. A summary of the results obtained from the three tufa samples is presented in Table 5.

Since calcareous tufa cannot be considered as closed systems, the obtained corrected dating should be treated as rough age estimates. The two samples collected from the thick tufa deposit capping the terrace of the Alfambra River in the footwall of Concud Fault yielded corrected ages of 285.2 ± 14 ka and 228.4 ± 11.4 ka. These age estimates are older than those obtained by Arlegui et al. (2006) from the same unit (169 ± 10 ka and 116 ± 4 ka). These authors neither indicate the applied analytical technique nor the sample amount range required for each determination, and therefore their published ages cannot be comparable with the one obtained in our work. The new dates obtained in our investigation provide an update of the tufa ages, which compare well with those reported by Gutiérrez et al. (2008) (250 + 32/-25 ka and 213 + 33/-26 ka) based on a multicollection technique for the isotope ratio determinations.

5.4. Radiocarbon dating

The radiocarbon samples collected from the two youngest fissure fills associated with Concud Fault (FF2 and FF3) have provided calibrated age ranges of 2344–2155 cal BP and 7972-7851 cal BP (error margin at 2 σ), respectively (Fig. 2 and Table 6). These ages are not in correct stratigraphic order. Gutiérrez et al. (2020b) indicated that the youngest age obtained from fissure FF2 could be related to contamination and that the age of FF3 could be a good approximation to the most recent faulting event recorded in this exposure. The UAM Luminescence Lab provided much older ages for the short-transport colluvial deposits of these fissures (38.6 ± 2.3 ka and 32.1 ± 2.4 ka; Lafuente et al. (2011). The radiocarbon age from the colluvium that truncates the fault at Cociero site (7589-7486 cal BP) (Fig. 3 and Table 6) is also much younger than the OSL age of the UAM Luminescence Lab (14.9 ± 1 ka; Lafuente et al., 2011).

6. Discussion

6.1. Refining the chronology of deposits associated with quaternary faults in the central sector of the Iberian Chain

Neotectonic and paleoseismological studies in the central sector of the Iberian Chain have gone through two main eras. In the first period, the published work was mainly focused on the identification of faulted Pliocene and Quaternary deposits, and the assessment of their displacement. The chronology of the Pliocene deposits was based on biostratigraphic data (e.g., Mein et al., 1989), whereas the relative age of the Quaternary deposits, mainly terraces and mantled pediments, where referred to the local morpho-stratigraphic scheme of alluvial levels. Traditionally, there was a tendency to identify four terrace levels correlative to the Alpine glaciations (e.g., Moissenet, 1985), leading to erroneous correlations and offset over-estimates (Gutiérrez et al., 2020b). More recent studies, based on larger-scale mapping revealed a larger number of terrace levels in most fluvial systems (Gutiérrez, 1998; Gutiérrez et al., 2020b). In a second era, the application of geochronological methods provided the opportunity to assess slip rates. Moreover, the concept of differentiating surface-faulting events attributable to paleoearthquakes was applied for the first time in Gutiérrez et al. (2005). This reveals the late commence of paleoseismic studies in the Iberian Chain.

The first slip rate estimates using numerically dated Quaternary deposits were provided for Concud Fault at Los Baños site. These slip rates were based on U/Th ages from tufa deposits at the footwall and the assumption that those deposits are correlative to a tufa layer in the downthrown block with markedly different thickness and facies (Arlegui et al, 2005, 2006; Simón et al., 2005) (Fig. 2). Subsequently, the number of numerical ages increased very rapidly, concurrently with the number of paleoseismological investigations aimed at assessing the seismic hazard associated with the faults. However, the new ages were TL datings provided by the now closed commercial UAM Luminescence Lab, lacking any cross-checking with other methods or laboratories. These geochronological data, together with the inferences derived from them, raised serious questions due to a number of inconsistencies difficult to conciliate with the regional geomorphological and neotectonic context: extremely high fluvial downcutting rates, anomalously high fault-slip rates, difficult-to-justify low earthquake recurrences and highly divergent ages for the same terrace or pediment level. The new ages obtained by our multi-method dating approach carried out at the CENIEH confirm the underestimation of the ages of the UAM Luminescence Lab and allow to preliminarily reassess the slip rates of some Quaternary faults in the Iberian Chain, a critical parameter for seismic hazard assessment.

6.1.1. The Concud-Teruel Fault

At Los Baños site (Fig. 2), two samples from the upper tufa unit of the Alfambra river terrace (+60–66m) were dated by U/Th series at 169 ± 10 ka and 116 ± 4 ka (Arlegui et al, 2005, 2006). Gutiérrez et al. (2008) published new overlapping U/Th series ages of 250 + 32/-25 ka and 213 + 33/-26 ka for the tufa unit and suggested than the terrace deposit was older that the ages obtained in previous studies. The two samples collected from the upper tufa unit in this work have provided minimum corrected U/Th series ages of >285 ± 14 ka and 228 ± 11 ka, which are consistent with those obtained by Gutiérrez et al. (2008). The ESR sample, collected from a sand bed intercalated within the lower detrital unit of this terrace, yielded an age estimate of 327 ± 31 ka. In the downthrown block, the five ESR, TT-OSL (MAM) and U/Th samples collected in this study provided ages between 3 and 6 times older than the TL datings previously obtained by the UAM Luminescence Lab for the same units (Fig. 2). In the lower package (PI), the unit I1 has been dated at 113.6 ± 7.3 ka by the UAM Luminescence Lab while our ESR sample yielded an age of 480 ± 44 ka. The tufa layer I3 and the overlying fine-grained detrital unit I4 have been dated by U/Th series at >388 ± 10 ka and by TT-OSL at 277 ± 35 ka, respectively. This new TT-OSL age estimate is significantly older than the TL age provided by the UAM Luminescence Lab (71.7 ± 5.2 ka) (Gutiérrez et al., 2008), although it should be taken with caution due to low number of aliquots involved in the D_E calculation. The three new ages obtained in this work using ESR,

Table 5
Measurements and age estimates obtained from the analyzed tufa samples collected at Los Baños site. Values in parenthesis indicate the 2σ uncertainty. Decay constants used in the calculations: λ238 = 1.55125x10-10; λ234 = 2.82206x10-6; λ230 = 9.1705x10-6 (from Cheng et al., 2013).

ID	^{238}U	^{230}Th	$^{230}Th/^{232}Th$	$\delta^{234}U$	$\delta^{234}U_{init}$	$^{230}Th/^{238}U$	^{230}Th	^{230}Th corr
Sample	[μg g^{-1}]	[μg g^{-1}]	x 10^{-6} [at/at]	[meas]	[calc]	[Bq/Bq]	[yr]	[yr]
T-BA-SU-1	0.746 ± 0.003	0.070 ± 0.003	214 ± 1	244 ± 2.5	546 ± 20	1.210 ± 0.003	337 750 ± 16 900	285 182 ± 14 250
T-BA-SU-2	0.270 ± 0.003	0.048 ± 0.003	124 ± 1	276 ± 2.5	525 ± 29	1.225 ± 0.003	256 567 ± 12 828	228 432 ± 11 425
T-BA-SU-3	0.688 ± 0.001	0.154 ± 0.003	97 ± 2	262 ± 2.3	782 ± 2	1.324 ± 0.003	391 527 ± 9450	387 754 ± 9526

Table 6
Radiocarbon samples dated by accelerator mass spectrometry. Sample code, laboratory number provided by Beta Analytic, material, conventional ages and calibrated ages with error margins of 1σ and 2σ calculated using the high probability density range method (BetaCal3.21) and the database Intcal13 (Reimer et al., 2013).

Code	Laboratory number	Material	Conventional age ^{14}C (yr BP)	Calibrated age (1σ) (yr BP)	Calibrated age (2σ) (yr BP)
T-CO-1712	Beta - 512900	organic sediment	6670 ± 30	7542 - 7512 (41.6%) 7578–7558 (26.6%)	7589–7486 (95.4%)
T-BAN-1707	Beta – 471194	organic sediment	2250 ± 30	2239–2181 (43.7%) 2333–2304 (24.5%)	2270–2155 (64.1%) 2344–2296 (31.3%)
T-BAN-1706	Beta - 471193	organic sediment	7090 ± 30	7959–7927 (41.5%) 7895 - 7871 (26.7%)	7972–7851 (95.4%)

TT-OSL and U–Th for the Lower Package (PI) are consistent with each other and with the geological context suggesting that the lower package of the downthrown block is not correlative and is much older than the footwall terrace (Gutiérrez et al., 2020b).

In the upper package (PII), the new samples collected yielded ESR ages (372 ± 29 ka and 198 ± 16 ka) much older than the corresponding previous TL ages (64.2 ± 4.4 ka and 62.4 ± 6.6 ka, respectively). However, the two radiocarbon samples collected from the youngest fissure fills (FF2 and FF3) made up of short-transport deposits have yielded ages of 2344–2155 cal BP and 7942–7851 cal BP, much younger than the corresponding previous TL ages (38.6 ± 2.3 ka and 32.1 ± 2.4 ka, respectively). The reverse order of these radiocarbon ages is attributed to contamination in the intermediate fissure FF2.

At Cociero site, located 1.1 km SSE of Los Baños site, we obtained an OSL age four times higher (60 ± 2 ka) than those obtained by the UAM Luminescence Lab (15.0 ± 0.9 ka and 15.6 ± 1.3 ka) for the upper fine-grained unit of the terrace (Gutiérrez et al., 2008; Lafuente et al., 2011). As in the case of Los Baños site, the new radiocarbon age obtained from the non-deformed and poorly sorted colluvium that truncates the fault (7589–7486 cal BP) is younger than the TL age provided by the UAM Luminescence Lab (14.9 ± 1.0 ka).

At Matauetа site, located around 300 m north of the Cociero site, Ezquerro et al. (2014) investigated a trench in a mantled pediment and published ten TL ages from the UAM Luminescence Lab ranging between 12.8 and 27.6 ka. According to Ezquerro et al. (2014) the ages derived from samples collected at both sides of the fault exposed in the trench lack consistency. The authors decided to use the six ages obtained from the downthrown block arguing a rejuvenation of the TL ages from the footwall related to erosion and reworking processes. The new OSL sample collected in this work yielded an age significantly older (87 ± 3 ka) than the ten ages provided by the UAM Luminescence Lab for the same pediment deposit. In addition, this new OSL age is consistent with our OSL age obtained for the terrace deposits exposed at the Cociero site (60 ± 2 ka), which corresponds to a younger morpho-stratigraphic unit.

At Pitarque site, Simón et al. (2017) investigated two trenches dug in a terrace of the Valdelobos Stream perched around 60 m above the current channel. These authors published six TL ages from this terrace provided by the UAM Luminescence Lab, ranging from 78.3 to 46.5 ka, and decided to use the youngest one for the estimation of slip rates. The new ESR sample collected from a sand bed intercalated within the same terrace has yielded an age of 307 ± 25 ka. The ages estimated by the UAM Luminescence Lab (Simón et al., 2017) are incongruously young compared to those obtained from nearby terraces of the Alfambra River at similar heights above the current channel. For instance, the +60–66 m terrace deposit at Los Baños site has been dated in this work by ESR at 327 ± 31 ka, while the Cuesta de la Bajada archeo-paleontological site, located in a +55 m terrace would be correlated to either MIS 7 or 9 (i.e., 243–337 ka; (Lisiecki and Raymo, 2005). This chronology has been established using a combination of OSL (293 ± 24 ka, 264 ± 22 ka and 281 ± 32 ka), ESR (350 ± 49 ka and 264 ± 42 ka) and Amino Acid Racemization (AAR) (431 ± 44 ka) dating (Duval et al., 2017a; Santonja et al., 2014).

6.1.2. The Daroca Fault

The Daroca Fault clearly ruptures a mantled pediment deposit in a quarry located 1.5 km south of Daroca town. This unit was dated by the UAM Luminescence Lab at 118.7 ± 16.2 ka and 112.8 ± 9.1 ka (Gutiérrez et al., 2008). However, the new sample collected from the same unit in this work has yielded a much older ESR age of 329 ± 43 ka.

6.1.3. The munébrega W fault

Gutiérrez et al. (2009) investigated a trench excavated across a 6–7 m high upslope-facing scarp generated by the Munébrega W Fault on a mantled pediment, with merges with a terrace of the Jalón River situated 45 m above the thalweg. These authors published various ages provided by the UAM Luminescence Lab from different units accumulated in the sediment trap associated with the antislope scarp (41, 32, 19 and 10 ka) and from the pre-deformation mantled pediment (71.8 ± 5.5 ka). A new sample collected from this pediment deposit has yielded a much older ESR age estimate of 241 ± 50 ka.

6.2. How reliable are the ages of the UAM luminescence lab?

The previous ages estimated by the UAM Luminescence Lab at the Concud-Teruel (Los Baños, Pitarque, Cociero and Matauetа sites), Daroca and Munébrega W faults show two clear trends. First, they are systematically 6–3 times younger than the new ESR-OSL-U/Th ages obtained in this work. The only exception are the new radiocarbon ages that are younger than the previous TL ages, all of them derived from colluvial facies, including two fissure fills. Second, they show an anomalous concentration around 46 ± 29 ka (mean ± 1sd). This temporal clustering is obtained considering all the TL ages from the UAM Luminescence Lab published in studies on faults of the Iberian Chain (Fig. 10). The application of a TL protocol used for dating ceramics instead of luminescence dating methods specific from sediments could explain the systematic large deviation that exists between the ages provided by the UAM Luminescence Lab and the more consistent ones presented in this work (See Section 3.1. and Table SD1 **in Supplementary Data**). Overall, the new ages presented in this paper have a more scattered temporal distribution coherent with the diverse morphostratigraphic position of the sampled units, and strongly suggest that the UAM Luminescence Lab significantly underestimate the age of the deposits (Fig. 10).

The main problem we faced when carrying out this work was the lack of information about the analyses performed by the UAM Luminescence Laboratory. Simple publication of dates alone is quite inadequate. To assess whether the ages are meaningful, reports from specialized luminescence laboratories and, most importantly, scientific publications including those ages should provide sufficient information on the following aspects, at least as freely accessible supplementary data (Duller, 2008; Duval et al., 2017b): (1) sample details such as a brief description of the sampling technique, photographs showing sampling locations, the depth below the current ground surface or stratigraphic and contextual relationships (Moreno et al., 2017; Nelson et al., 2015); (2) laboratory procedures used to prepare samples, the equipment used to make measurements or the details of rejection criteria undertaken; (3) the methods used for dose rate measurements, differentiating clearly between *in situ* and laboratory measurements; (4) graphs showing examples of the luminescence signal measured, tables of results including sampling depth, water content values, grain size, U, Th and K contents,

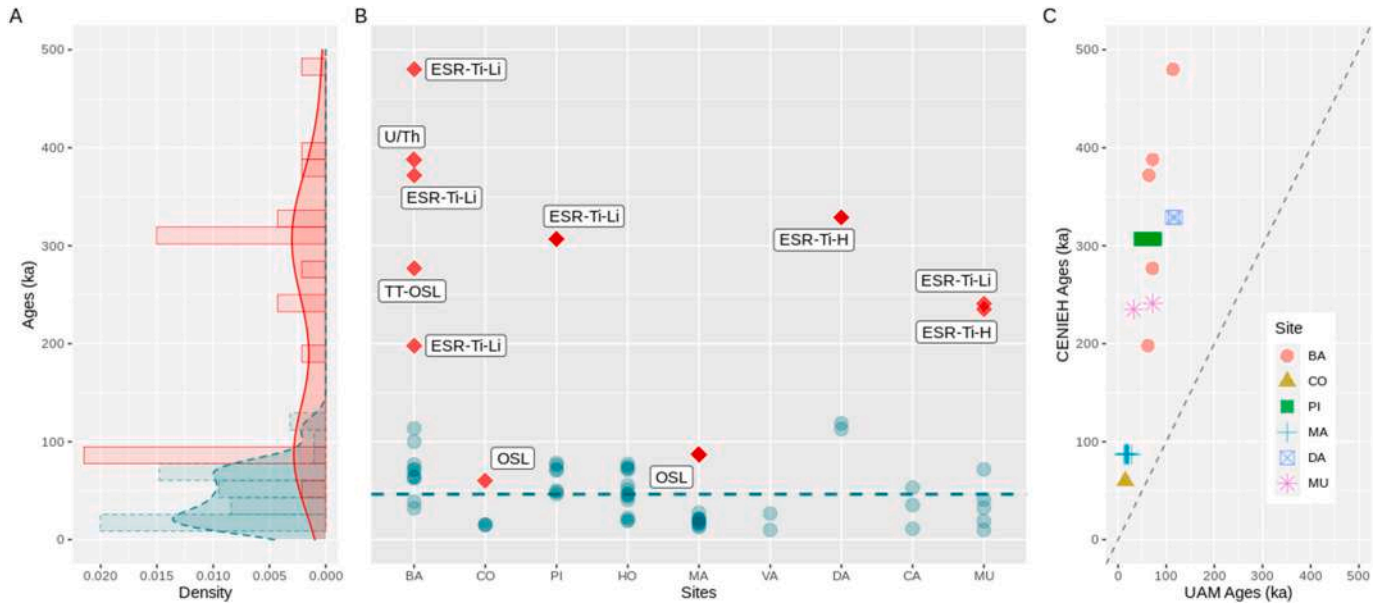

Fig. 10. Ages obtained in this work at the CENIEH's Geochronology laboratories *(red squares)* versus the 55 previously published UAM Luminescence Lab ages *(cyan circles)* from different sites associated with the Concud-Teruel, Calamocha, Daroca and Munébrega W Faults in the central sector of the Iberian Chain. (A) Frequency density histograms and density plot of the ages represented in B. The 500 ka time period is divided into 30 equal bins. UAM Luminescence Lab ages are depicted with dashed lines. (B) Scatterplot showing that the ages of the UAM Luminescence Lab are systematically younger than those of the CENIEH and are concentrated at around 46 ± 29 ka (mean ± 1σ; cyan horizontal dashed line). Dating methods are represented as labels in the CENIEH's ages. (C) Scatterplot representing new CENIEH ages versus previous TL ages of the UAM Luminescence Lab for the same stratigraphic unit. BA: Los Baños (Gutiérrez et al., 2008; Lafuente et al, 2010, 2011); CO: Cociero (Gutiérrez et al., 2008; Lafuente et al, 2011, 2014); PI: Pitarque (Simón et al, 2012, 2017); HO: Hocino (Lafuente et al, 2010, 2014); MA: Matauleta (Ezquerro et al., 2014; Simón et al., 2016); VA: Valdelobos (Simón et al, 2012, 2017); DA: Daroca (Gutiérrez et al, 2008, 2020a); CA: Calamocha (Martín-Bello et al., 2014); MU: Munébrega (Gutiérrez et al., 2009).

equivalent doses (D_E), dose rate (D) etc, (Duller, 2008; Duval et al., 2017b; Wintle and Huntley, 1982). As far as we know, none of these aspects have been published or provided by the commercial UAM Luminescence Lab in their reports (Gutiérrez et al., 2008; Lafuente et al, 2011, 2014; Martín-Bello et al., 2014; Simón et al, 2012, 2016, 2017).

Considering all these issues, we seriously question the reliability of the ages provided by the UAM Luminescence Lab. Even though they mention calculating OSL ages in several published papers, optical stimulation was never applied to their samples, and as mentioned in Section 3.1., the TL *"fine grain"* method (Zimmerman, 1971) was systematically performed. As we have explained in Section 6.1., the proposed lack of validity of the TL ages of the UAM Luminescence Lab is also supported by a number of inconsistencies and anomalous parameters derived from them. Thus, the UAM Luminescence Lab ages published and used by many authors from multiple research fields during the last two decades in Spain cannot be properly validated and all previous published ages should be considered with caution.

6.3. Geomorphological and seismic hazard implications

The fact that the new ages obtained by different methods (ESR, OSL, U/Th) for Quaternary terraces and pediments associated with active faults are 3–6 times older than the previous and questionable ages of the UAM Luminescence Lab, has important implications for landscape-evolution studies and seismic hazard assessments. The new ages strength the need of abandoning old and simplified morphostratigraphic schemes based on 3–4 alluvial levels, and the importance of producing new geomorphological maps including complete terrace and pediment morphosequences. This is essential for avoiding misleading correlations, potentially resulting in erroneous displacement estimates, and for preventing chronological contradictions. For instance, Simón et al. (2017; Table 1), differentiates four terrace levels in the Alfambra-Turia fluvial system, but the two intermediate terraces are split into 2–3 sublevels. Moreover, the faulted terrace sublevel at Pitarque site has received difficult-to-conciliate ages from the UAM Luminescence Lab of 90.5 ka, 76 ka, and 78.3–46.5 ka, but the authors decide to use the youngest one for estimating a slip rate for the Teruel Fault (Simón et al., 2017 and references therein). An ESR age of 307 ± 25 ka has been obtained for that terrace at Pitarque site in this work, and detailed mapping presented in Gutiérrez et al. (2020b) reveals that it is not a terrace of the Turia River, but of a tributary stream, which shows a sequence of eight terrace levels.

As discussed in Gutiérrez et al. (2020b), the young TL ages of terrace deposits provided by the UAM Luminescence Lab implicitly indicate anomalously high fluvial downcutting rates above 0.5 mm/a, with difficult-to-justify extreme values as high as 1.3 mm/a (e.g. terrace at Pitarque site). These values are not consistent with numerous studies conducted in central and eastern Spain that provide long-term incision rates below 0.2 mm/a for multiple fluvial systems and using various methods (Benito-Calvo et al, 1998, 2018; Giachetta et al., 2015; Moreno et al., 2012; Ortiz et al., 2009; Sancho et al., 2016; Silva et al., 2017). The new ages, although limited and obtained from deformed deposits that have experienced some post-sedimentary vertical displacement, indicate downcutting rates within the range of 0.1–0.3 mm/a, consistent with the specific literature on the subject (Gutiérrez et al., 2020b).

Some of the main parameters used to characterize fault sources in probabilistic seismic hazard analyses rely upon geochronological data: slip rates, number and timing of paleoearthquakes, including the MRE, and earthquake recurrence. Obviously, the data derived from the TL ages of the UAM Luminescence Lab have questionable validity and most probably result in significant hazard overestimates, given that they correspond to minimum ages far from the actual ones. This is supported by cross-checking those hazard parameters with various types of data independent from the ages of the UAM Luminescence Lab. As discussed in Gutiérrez et al. (2020b), the long-term slip rates estimated using the TL ages of the UAM Luminescence Lab, with values as high as 0.29 mm/a (e.g., Concud Fault; Simón et al., 2016), are significantly higher than: (1) those calculated for the same faults using Pliocene limestones (≤0.1

mm/a); (2) the slip rates estimated for some Quaternary faults in the Iberian Chain using radiocarbon ages (0.05–0.07 mm/a in Rubielos de la Cérida Fault; Gutiérrez et al., 2008) or recent OSL ages from a non-commercial lab (0.05 mm/a in Valdecebro Fault (Simón et al., 2019); and (3) the slip rates estimated for normal faults in the Catalan Coastal Ranges in NE Spain, related to the same geotectonic mechanism (i.e., post-orogenic extension on the western margin of the Valencia Trough; Perea et al., 2012). A similar discrepancy is observed in this latter region, where most of the faults have slip rates below 0.1 mm/a (Perea et al., 2012), with only one outlier (0.26–0.3 mm/a; Torreblanca Fault), which corresponds to the only fault characterized using geochronological data from the UAM Luminescence Lab (Simón et al., 2013). In contrast, slip rates estimated for the different faults (Gutiérrez et al., 2020b) with the new geochronological data presented in this work indicate slip rates 6.6–2.7 times lower than those derived from the ages of the UAM Luminescence Lab, and consistent with the published literature independent of those questionable TL ages (See further discussion in Gutiérrez et al., 2020b).

The debatable reliability of the TL ages from the UAM Luminescence Lab also generates serious concerns about the validity of the paleoseismic histories inferred for some faults from multiple trenches, and the hazard parameters derived from their integration. The numerical ages provide the basis for correlating/differentiating paleoearthquakes, establishing the paleoseismic history, bracketing the age of the events, and estimating average earthquake recurrence. The societal impact of the estimates derived from the ages of the UAM Luminescence Lab is illustrated by a seismic hazard analysis which induced the stoppage and re-design of the construction of the Hospital of Teruel in the vicinity of Concud Fault. This hazard analysis incorporated as seismic sources (Simón et al., 2016): (1) an earthquake catalog from a relatively large area (ca. 75 × 75 km), without applying attenuation laws; and (2) the Concud Fault as the control fault source, considering that it has experienced 11 surface faulting events since 74 ka (average recurrence 7–8 ka), with the MRE constrained at 12.8–3.4 ka, and a slip rate of 0.29 mm/a. However, the new ages strongly suggest that the Concud Fault has a much lower seismogenic potential, with significantly higher slip rate and recurrence (Gutiérrez et al., 2020b).

7. Conclusions

The multi-method dating approach applied to Quaternary deposits associated with active faults in the central sector of the Iberian Chain (NE Spain), has provided a new set of numerical ages for assessing the validity of the ages previously obtained by the commercial UAM Luminescence Lab. The new ages strongly challenge the reliability of the previous geochronological data and provide a preliminary basis for re-assessing the previously overestimated slip rate of the faults and the long-term incision rates of the fluvial systems. The main conclusions of this investigation can be summarized as follows:

1) The new ESR, OSL and U/Th numerical ages obtained by the CENIEH's Geochronology Laboratory are systematically 6 to 3 times older than the previous ones provided by the UAM Luminescence Lab. The latter show an anomalous concentration around 46 ± 29 ka (mean ± 1sd). Very few details of the methodology applied by the UAM Luminescence Lab have been published. However, although they used to deliver succinct reports indicating the calculation of OSL ages, optical stimulation was never applied to their samples. It appears that this laboratory used the TL *"fine grain"* method (Zimmerman, 1971) for sediments just as it was used for pottery. This could explain the systematically large deviation between the anomalously young ages provided by the UAM Luminescence Lab and the more consistent ones presented in this work.
2) The reliability of the ages provided by the UAM Luminescence Lab is seriously questioned. The lack of information on important aspects such as the sampling technique, laboratory sample preparation procedures, equipment used to make measurements, details on rejection criteria, methods applied to calculate the dose rate, and graphs or tables of results, prevents the evaluation of the technique applied and the ages obtained. Thus, previous ages from the UAM Luminescence Lab used by many authors to make interpretations on various geological and archaeological issues during the last two decades in Spain cannot be properly validated and should be considered with caution.
3) The use of unreliable ages for the characterization of fault sources in the central sector of the Iberian Chain has led to erroneous seismic hazard assessments with significant societal and economic impact, such as those that induced the interruption of the construction of a new hospital in Teruel city (Simón et al., 2016). Hopefully, the new data will contribute to alert about the need for new geochronological studies and hazard assessments.
4) The multi-dating approach has demonstrated its potential to cross-checking the validity of the available numerical ages, to identify systematic biases and to take decisions about anomalous ages. This work has also highlighted the need to review the ages of other locations in the region, ideally using this approach, to refine the chronology of Quaternary studies and hazard analyses.

Declaration of competing interest

The authors declare that they have no known competing financial interests or personal relationships that could have appeared to influence the work reported in this paper.

Acknowledgments

This work has been supported by the project CGL2017-85045-P (Ministerio de Ciencia, Innovación y Universidades, Gobierno de España). Authors would like to thank Mario Modesto-Mata for his invaluable help in the creation of Fig. 10 and Isabel Sarró for her support in the coordination of this project. We thank the two anonymous reviewers for their useful comments and extremely detailed revision.

Appendix A. Supplementary data

Supplementary data to this article can be found online at https://doi.org/10.1016/j.quageo.2021.101185.

References

Adamiec, G., Duller, G.A.T., Roberts, H.M., Wintle, A., 2010. Improving the TT-OSL SAR protocol through source trap characterisation. Radiat. Meas. 45, 768–777. https://doi.org/10.1016/j.radmeas.2010.03.009.

Aitken, M.J., 1989. Luminescence dating: a guide for non-specialist. Archaeometry 31, 147–159. https://doi.org/10.1111/j.1475-4754.1989.tb01010.x.

Aitken, M.J., Xie, J., 1990. Moisture correction for annual gamma dose. Ancient TL 8, 6–9.

Arlegui, L.E., Simón, J.L., Lisle, R.J., Orife, T., 2006. Analysis of non-striated faults in a recent extensional setting: the Plio-Pleistocene Concud fault (Jiloca graben, eastern Spain). J. Struct. Geol. 28, 1019–1027. https://doi.org/10.1016/j.jsg.2006.03.009.

Arlegui, L.E., Simón, J.L., Lisle, R.J., Orife, T., 2005. Late Pliocene–Pleistocene stress field in the Teruel and Jiloca grabens (eastern Spain): contribution of a new method of stress inversion. J. Struct. Geol. 27, 693–705. https://doi.org/10.1016/j.jsg.2004.10.013.

Arnold, L.J., Demuro, M., 2015. Insights into TT-OSL signal stability from single-grain analyses of known-age deposits at Atapuerca, Spain. Quat. Geochronol. 30, 472–478. https://doi.org/10.1016/j.quageo.2015.02.005.

Barandiarán, I., Benéitez, P., Cava, A., Millán, M.A., 2007. The Gravettian flint workshop of Mugarduia sur (Navarra): identification and chronology. Zephyrus 60, 15–26.

Bartz, M., Rixhon, G., Duval, M., King, G.E., Álvarez Posada, C., Parés, J.M., Brückner, H., 2018. Successful combination of electron spin resonance, luminescence and palaeomagnetic dating methods allows reconstruction of the Pleistocene evolution of the lower Moulouya river (NE Morocco). Quat. Sci. Rev. 185, 153–171. https://doi.org/10.1016/j.quascirev.2017.11.008.

Benito-Calvo, A., Ortega, A.I., Navazo, M., Moreno, D., Pérez-González, A., Parés, J.M., Bermúdez de Castro, J.M., Carbonell, E., 2018. Evolución geodinámica pleistocena del valle del río Arlanzón: implicaciones en la formación del sistema endokárstico y

los yacimientos al aire libre de la Sierra de Atapuerca (Burgos, España). BG 1129, 59–82. https://doi.org/10.21701/bolgeomin.129.1.003.
Benito-Calvo, A., Pérez-González, A., Santonja, M., 1998. Terrazas rocosas, aluviales y travertínicas del valle alto del río Henares (Guadalajara, España). Geogaceta 24, 55–58.
Brennan, B.J., 2003. Beta doses to spherical grains. Radiat. Meas. 37, 299–303. https://doi.org/10.1016/S1350-4487(03)00011-8.
Brennan, B.J., Lyons, R.G., Phillips, S.W., 1991. Attenuation of alpha particle track dose for spherical grains. Int. J. Radiat. Appl. Instrum. Nucl. Tracks Radiat. Meas. 18, 249–253. https://doi.org/10.1016/1359-0189(91)90119-3.
Burbank, D.W., Anderson, R.S., 2012. Tectonic Geomorphology. Wiley-Blackwell, Chichester.
Burillo, F., Gutiérrez, M., Peña, J.L., 1985. Datación arqueológica de deformaciones tectónicas en vertientes holocenas de sierra Palomera (Cordillera Ibérica centroriental). In: Actas de La I Reunión Del Cuaternario, pp. 355–366. Lisboa.
Calderón, T., Arriba, J.G., Millán, A., Blasco, C., 1988. Servicio de datación absoluta por termoluminiscencia y analítica de cerámicas arqueológicas en la Universidad Autónoma de Madrid. CuPAUAM 15, 385–397. https://doi.org/10.15366/cupauam1988.15.014.
Carbonel, D., Gutiérrez, F., Sevil, J., McCalpin, J.P., 2019. Evaluating Quaternary activity versus inactivity on faults and folds using geomorphological mapping and trenching: seismic hazard implications. Geomorphology 338, 43–60. https://doi.org/10.1016/j.geomorph.2019.04.015.
Chapot, M.S., Roberts, H.M., Duller, G.A.T., Lai, Z.P., 2016. Natural and laboratory TT-OSL dose response curves: Testing the lifetime of the TT-OSL signal in nature. Radiat. Meas. 85, 41–50. https://doi.org/10.1016/j.radmeas.2015.11.008.
Cheng, H., Lawrence Edwards, R., Shen, C.-C., Polyak, V.J., Asmerom, Y., Woodhead, J., Hellstrom, J., Wang, Y., Kong, X., Spötl, C., Wang, X., Calvin Alexander, E., 2013. Improvements in ^{230}Th dating, ^{230}Th and ^{234}U half-life values, and U–Th isotopic measurements by multi-collector inductively coupled plasma mass spectrometry. Earth Planet Sci. Lett. 371–372, 82–91. https://doi.org/10.1016/j.epsl.2013.04.006.
Cortés Gracia, Á.L., Casas-Sainz, A.M., 1996. Deformación alpina de zócalo y cobertera en el borde norte de la cordillera Ibérica (Cubeta de Azuara - sierra de Herrera). Rev. Soc. Geol. Espana 9, 51–66.
De Vicente, G., Vegas, R., Cloetingh, S., Muñoz Martín, A., Álvarez, J., González-Casado, J.M., Heredia, N., Rodríguez-Fernández, L.R., Guimerà, J., Casas, A., 2005. Iberian foreland Cenozoic Ranges: a reologic-cinematic classifitacion. In: Geophysical Research Abstract. European Geosciences Union.
Debenham, N.C., 1985. Use of U.V. emissions in TL dating of sediments. Nucl. Tracks Radiat. Meas. 10, 717–724. https://doi.org/10.1016/0735-245X(85)90080-8, 1982.
Dietze, M., Kreutzer, S., Burow, C., Fuchs, M.C., Fischer, M., Schmidt, C., 2016. The abanico plot: visualising chronometric data with individual standard errors. Quat. Geochronol. 31, 12–18. https://doi.org/10.1016/j.quageo.2015.09.003.
Duller, G.A.T., 2015. The Analyst Software Package for Luminescence Data: Overview and Recent Improvements 33, p. 8.
Duller, G.A.T., 2008. Luminescence Dating: Guidelines on Using Luminescence Dating in Archaeology (English Heritage, Swindon).
Duller, G.A.T., 2004. Luminescence dating of quaternary sediments: recent advances. J. Quat. Sci. 19, 183–192. https://doi.org/10.1002/jqs.809.
Duller, G.A.T., 2003. Distinguishing quartz and feldspar in single grain luminescence measurements. Radiat. Meas. 37, 161–165. https://doi.org/10.1016/S1350-4487(02)00170-1.
Durcan, J.A., King, G.E., Duller, G.A.T., 2015. DRAC: dose rate and age calculator for trapped charge dating. Quat. Geochronol. 28, 54–61. https://doi.org/10.1016/j.quageo.2015.03.012.
Duval, M., Arnold, L.J., 2013. Field gamma dose-rate assessment in natural sedimentary contexts using $LaBr_3$(Ce) and NaI(Tl) probes: a comparison between the “threshold” and “windows” techniques. Appl. Radiat. Isot. 74, 36–45. https://doi.org/10.1016/j.apradiso.2012.12.006.
Duval, M., Arnold, L.J., Guilarte, V., Demuro, M., Santonja, M., Pérez-González, A., 2017a. Electron spin resonance dating of optically bleached quartz grains from the Middle Palaeolithic site of Cuesta de la Bajada (Spain) using the multiple centres approach. Quat. Geochronol. 37, 82–96. https://doi.org/10.1016/j.quageo.2016.09.006.
Duval, M., Bahain, J.-J., Bartz, M., Falguères, C., Guilarte, V., Moreno, D., Tissoux, H., del Val, M., Voinchet, P., Arnold, L.J., 2017b. Defining minimum reporting requirements for ESR dating of optically bleached quartz grains. Ancient TL 35, 11–19.
Duval, M., Grün, R., Falguères, C., Bahain, J.-J., Dolo, J.-M., 2009. ESR dating of Lower Pleistocene fossil teeth: limits of the single saturating exponential (SSE) function for the equivalent dose determination. Radiat. Meas. 44, 477–482. https://doi.org/10.1016/j.radmeas.2009.03.017.
Duval, M., Guilarte, V., 2015. ESR dosimetry of optically bleached quartz grains extracted from Plio-Quaternary sediment: evaluating some key aspects of the ESR signals associated to the Ti-centers. Radiat. Meas. 78, 28–41. https://doi.org/10.1016/j.radmeas.2014.10.002.
Duval, M., Sancho, C., Calle, M., Guilarte, V., Peña-Monné, J.L., 2015. On the interest of using the multiple center approach in ESR dating of optically bleached quartz grains: some examples from the Early Pleistocene terraces of the Alcanadre River (Ebro basin, Spain). Quat. Geochronol. 29, 58–69. https://doi.org/10.1016/j.quageo.2015.06.006.
Duval, M., Voinchet, P., Arnold, L.J., Parés, J.M., Minnella, W., Guilarte, V., Demuro, M., Falguères, C., Bahain, J.-J., Despriée, J., 2020. A multi-technique dating study of two lower palaeolithic sites from the cher valley (Middle Loire catchment, France): Lunery-la Terre-des-Sablons and Brinay-la Noira. Quaternary International S1040618220302664. https://doi.org/10.1016/j.quaint.2020.05.033.
Ezquerro, L., Liesa, C.L., Simón, J.L., Arlegui, L.E., Luzón, A., Lafuente, P., 2014. Correlation of sedimentary units from grain-size and mineralogic analyses as a tool for constraining trench interpretations in palaeoseismology. Int. J. Earth Sci. 103, 2327–2333. https://doi.org/10.1007/s00531-014-1079-5.
Galbraith, R.F., Roberts, R.G., 2012. Statistical aspects of equivalent dose and error calculation and display in OSL dating: an overview and some recommendations. Quat. Geochronol. 11, 1–27. https://doi.org/10.1016/j.quageo.2012.04.020.
Garnett, E.R., Gilmour, M.A., Rowe, P.J., Andrews, J.E., Preece, R.C., 2004. ^{230}Th/^{234}U dating of Holocene tufas: possibilities and problems. Quat. Sci. Rev. 23, 947–958. https://doi.org/10.1016/j.quascirev.2003.06.018.
Giachetta, E., Molin, P., Scotti, V.N., Faccenna, C., 2015. Plio-Quaternary uplift of the Iberian Chain (central–eastern Spain) from landscape evolution experiments and river profile modeling. Geomorphology 246, 48–67. https://doi.org/10.1016/j.geomorph.2015.06.005.
Gracia, F.J., Gutiérrez, F., Gutiérrez, M., 2003. The Jiloca karst polje-tectonic graben (Iberian Range, NE Spain). Geomorphology 52, 215–231. https://doi.org/10.1016/S0169-555X(02)00257-X.
Gracia Prieto, F.J., 1992. Tectónica pliocena de la Fosa de Daroca (prov. de Zaragoza). Geogaceta 11, 127–129.
Grün, R., 1994. A cautionary note: use of water content and depth for cosmic ray dose rate in AGE and DATA programs. Ancient TL 12, 50–51.
Grün, R., 1989. Electron spin resonance (ESR) dating. Quat. Int. 1, 65–109.
Guérin, G., Mercier, N., Adamiec, G., 2011. Dose-rate conversion factors: update. Ancient TL 29, 5–8.
Guimerà, J., 2018. Structure of an intraplate fold-and-thrust belt: the Iberian Chain. A synthesis. Geol. Acta 16, 427–438. https://doi.org/10.1344/GeologicaActa2018.16.4.6.
Gutiérrez, F., 1998. Fenómenos de subsidencia por disolución de formaciones evaporíticas en las fosas neógenas de Teruel y Calatayud (PhD). University of Zaragoza, Zaragoza.
Gutiérrez, F., Carbonel, D., Sevil, J., Moreno, D., Linares, R., Comas, X., Zarroca, M., Roqué, C., McCalpin, J.P., 2020a. Neotectonics and late holocene paleoseismic evidence in the plio-quaternary Daroca half-graben, iberian Chain, NE Spain. Implications for fault source characterization. J. Struct. Geol. 131, 103933. https://doi.org/10.1016/j.jsg.2019.103933.
Gutiérrez, F., Gracia, F.J., Gutiérrez, M., Lucha, P., Guerrero, J., Carbonel, D., Galve, J.P., 2012. A review on Quaternary tectonic and nontectonic faults in the central sector of the Iberian Chain, NE Spain. J. Iber. Geol. 38, 145–160. https://doi.org/10.5209/rev_JIGE.2012.v38.n1.39210.
Gutiérrez, F., Gracia, J., Gutiérrez, M., 2005. Karst, neotectonics and periglacial features in the Iberian Range. In: Desir, G., Gutiérrez, F., Gutiérrez, M. (Eds.), Sixth International Conference on Geomorphology. Field Trip Guides, pp. 343–397. Zaragoza.
Gutiérrez, F., Gutiérrez, M., Gracia, F.J., McCalpin, J.P., Lucha, P., Guerrero, J., 2008. Plio-Quaternary extensional seismotectonics and drainage network development in the central sector of the Iberian Chain (NE Spain). Geomorphology 102, 21–42. https://doi.org/10.1016/j.geomorph.2007.07.020.
Gutiérrez, F., Lucha, P., Jordá, L., 2013. The Río Grío depression (Iberian Chain, NE Spain). Neotectonic graben vs. fluvial valley. Cuaternario Geomorfol. 27, 5–32.
Gutiérrez, F., Masana, E., González, Á., Lucha, P., Guerrero, J., McCalpin, J.P., 2009. Late quaternary paleoseismic evidence on the Munébrega half-graben fault (iberian range, Spain). Int. J. Earth Sci. 98, 1691–1703. https://doi.org/10.1007/s00531-008-0319-y.
Gutiérrez, F., Moreno, D., López, G.I., Jiménez, F., del Val, M., Alonso, M.J., Martínez-Pillado, V., Guzmán, O., Martínez, D., Carbonel, D., 2020b. Revisiting the slip rate of Quaternary faults in the Iberian Chain, NE Spain. Geomorphic and seismic-hazard implications. Geomorphology 363, 107233. https://doi.org/10.1016/j.geomorph.2020.107233.
Hernandez, M., Mauz, B., Mercier, N., Shen, Z., 2012. Evaluating the efficiency of TT-OSL SAR protocols. Radiat. Meas. 47, 669–673. https://doi.org/10.1016/j.radmeas.2012.04.017.
Huntley, D.J., 1985. On the zeroing of the thermoluminescence of sediments. Phys. Chem. Miner. 12, 122–127. https://doi.org/10.1007/BF01046837.
Ivanovich, M., Harmon, R.S., 1992. Uranium-series Disequilibrium: Applications to Earth, Marine, and Environmental Sciences. Clarendon Press, Oxford, UK.
Kusiak, J., Lanczont, M., 2000. New results of TL dating of the loess profiles at Polanów Samborzecki with use of the optical filters BG-28 and UG-11. Geochronometria 19, 1–6.
Lafuente, P., 2011. Tectónica activa y paleosismicidad de la falla de Concud (Cordillera Ibérica central) (PhD). Universidad de Zaragoza, Zaragoza.
Lafuente, P., Arlegui, L.E., Liesa, C.L., Pueyo, Ó., Simón, J.L., 2014. Spatial and temporal variation of palaeoseismic activity at an intraplate, historically quiescent structure: the Concud fault (Iberian Chain, Spain). Tectonophysics 632, 167–187. https://doi.org/10.1016/j.tecto.2014.06.012.
Lafuente, P., Arlegui, L.E., Liesa, C.L., Simón, J.L., 2011. Paleoseismological analysis of an intraplate extensional structure: the Concud fault (Iberian Chain, eastern Spain). Int. J. Earth Sci. 100, 1713–1732. https://doi.org/10.1007/s00531-010-0542-1.
Lafuente, P., Arlegui, L.E., Liesa, C.L., Simón, J.L., 2010. Nuevo estudio paleosismológico en el sector central de la Falla de Concud (Fosa del Jiloca, Teruel): resultados preliminares. In: Martín-González, F., Insua-Arévalo, J.M. (Eds.), Contribución de la geología al análisis de la peligrosidad sísmica. I Reunión Ibérica sobre fallas activas y paleosismología, pp. 67–70.
Lisiecki, L.E., Raymo, M.E., 2005. A Pliocene-Pleistocene stack of 57 globally distributed benthic δ18O records. Paleoceanography 20. https://doi.org/10.1029/2004PA001071.

Martín-Bello, L., Arlegui, L.E., Ezquerro, L., Liesa, C.L., Simón, J.L., 2014. La falla de Calamocha (Fosa del Jiloca, Cordillera Ibérica): estructura y actividad pleistocena. In: Una aproximación multidisciplinar al estudio de las fallas activas, los terremotos y el riesgo sísmico. II Reunión Ibérica sobre fallas activas y paleosismología, pp. 55–58. Lorca.

Martínez-Aguirre, A., Alcaraz-Pelegrina, J.M., Rodríguez-Vidal, J., 2019. U/Th dating of impure carbonates: $^{230}Th/^{232}Th$ activity ratios in detrital material. J. Radioanal. Nucl. Chem. 321, 71–81. https://doi.org/10.1007/s10967-019-06560-3.

McCalpin, J. (Ed.), 2009. Paleoseismology, second ed. International geophysics series. Academic Press, Burlington, MA.

McCalpin, J.P., Gutierrez, F., Bruhn, R.L., Guerrero, J., Pavlis, T.L., Lucha, P., 2020. Tectonic geomorphology and late Quaternary deformation on the Ragged Mountain fault, Yakutat microplate, south coastal Alaska. Geomorphology 351, 106875. https://doi.org/10.1016/j.geomorph.2019.106875.

Mein, P., Moissenet, E., Adrover, R., 1989. Biostratigraphie du Néogène supérieur du bassin de Teruel. Paleontologia i Evolució 23, 121–139.

Méndez-Quintas, E., Santonja, M., Pérez-González, A., Duval, M., Demuro, M., Arnold, L. J., 2018. First evidence of an extensive Acheulean large cutting tool accumulation in Europe from Porto Maior (Galicia, Spain). Sci. Rep. 8, 3082. https://doi.org/10.1038/s41598-018-21320-1.

Moissenet, E., 1985. Le Quaternaire moyen alluvial du Fosse de Teruel. Physio-Géo 14, 61–78.

Moreno, D., Duval, M., Rubio-Jara, S., Panera, J., Bahain, J.J., Shao, Q., Pérez-González, A., Falguères, C., 2019. ESR dating of Middle Pleistocene archaeo-paleontological sites from the Manzanares and Jarama river valleys (Madrid basin, Spain). Quat. Int. 520, 23–38. https://doi.org/10.1016/j.quaint.2017.09.003.

Moreno, D., Falguères, C., Pérez-González, A., Duval, M., Voinchet, P., Benito-Calvo, A., Ortega, A.I., Bahain, J.-J., Sala, R., Carbonell, E., Bermúdez de Castro, J.M., Arsuaga, J.L., 2012. ESR chronology of alluvial deposits in the arlanzón valley (atapuerca, Spain): contemporaneity with atapuerca gran dolina site. Quat. Geochronol. 10, 418–423. https://doi.org/10.1016/j.quageo.2012.04.018.

Moreno, D., Richard, M., Bahain, J., Duval, M., Falguères, C., Tissoux, H., Voinchet, P., 2017. ESR dating of sedimentary quartz grains: some basic guidelines to ensure optimal sampling conditions. Quaternaire 28, 161–166. https://doi.org/10.4000/quaternaire.8008.

Murray, A.S., Wintle, A., 2000. Luminescence dating of quartz using an improved single-aliquot regenerative-dose protocol. Radiat. Meas. 32, 57–73. https://doi.org/10.1016/S1350-4487(99)00253-X.

Nelson, M.S., Gray, H.J., Johnson, J.A., Rittenour, T.M., Feathers, J.K., Mahan, S.A., 2015. User guide for luminescence sampling in archaeological and geological contexts. Adv. archaeol. pract. 3, 166–177. https://doi.org/10.7183/2326-3768.3.2.166.

Ortiz, J.E., Torres, T., Delgado, A., Reyes, E., Díaz-Bautista, A., 2009. A review of the Tagus river tufa deposits (central Spain): age and palaeoenvironmental record. Quat. Sci. Rev. 28, 947–963. https://doi.org/10.1016/j.quascirev.2008.12.007.

Perea, H., Masana, E., Santanach, P., 2012. An active zone characterized by slow normal faults, the northwestern margin of the València trough (NE Iberia): a review. J. Iber. Geol. 38, 31–52. https://doi.org/10.5209/rev_JIGE.2012.v38.n1.39204.

Porat, N., Duller, G.A.T., Roberts, H.M., Wintle, A., 2009. A simplified SAR protocol for TT-OSL. Radiat. Meas. 44, 538–542. https://doi.org/10.1016/j.radmeas.2008.12.004.

Prescott, J.R., Hutton, J.T., 1994. Cosmic ray contributions to dose rates for luminescence and ESR dating: large depths and long-term time variations. Radiat. Meas. 23, 497–500. https://doi.org/10.1016/1350-4487(94)90086-8.

Prescott, J.R., Hutton, J.T., 1988. Cosmic ray and Gamma ray dosimetry for TL and ESR. Nucl. Tracks Radiat. Meas. 14, 223–227.

Reimer, P.J., Bard, E., Bayliss, A., Beck, J.W., Blackwell, P.G., Ramsey, C.B., Buck, C.E., Cheng, H., Edwards, R.L., Friedrich, M., Grootes, P.M., Guilderson, T.P., Haflidason, H., Hajdas, I., Hatté, C., Heaton, T.J., Hoffmann, D.L., Hogg, A.G., Hughen, K.A., Kaiser, K.F., Kromer, B., Manning, S.W., Niu, M., Reimer, R.W., Richards, D.A., Scott, E.M., Southon, J.R., Staff, R.A., Turney, C.S.M., van der Plicht, J., 2013. IntCal13 and Marine13 radiocarbon age calibration curves 0–50,000 Years cal BP. Radiocarbon 55, 1869–1887. https://doi.org/10.2458/azu_js_rc.55.16947.

Rubio, J.C., Simón, J.L., 2007. Tectonic subsidence v. erosional lowering in a controversial intramontane depression: the Jiloca basin (Iberian Chain, Spain). Geol. Mag. 144, 127–141. https://doi.org/10.1017/S0016756806002949.

Sancho, C., Calle, M., Peña-Monné, J.L., Duval, M., Oliva-Urcia, B., Pueyo, E.L., Benito, G., Moreno, A., 2016. Dating the earliest pleistocene alluvial terrace of the alcanadre river (ebro basin, NE Spain): insights into the landscape evolution and involved processes. Quat. Int. 407, 86–95. https://doi.org/10.1016/j.quaint.2015.10.050.

Santonja, M., Pérez-González, A., Domínguez-Rodrigo, M., Panera, J., Rubio-Jara, S., Sesé, C., Soto, E., Arnold, L.J., Duval, M., Demuro, M., Ortiz, J.E., de Torres, T., Mercier, N., Barba, R., Yravedra, J., 2014. The Middle paleolithic site of Cuesta de la Bajada (Teruel, Spain): a perspective on the acheulean and Middle paleolithic technocomplexes in europe. J. Archaeol. Sci. 49, 556–571. https://doi.org/10.1016/j.jas.2014.06.003.

Silva, P.G., Roquero, E., López-Recio, M., Huerta, P., Martínez-Graña, A.M., 2017. Chronology of fluvial terrace sequences for large Atlantic rivers in the Iberian Peninsula (Upper Tagus and Duero drainage basins, Central Spain). Quat. Sci. Rev. 166, 188–203. https://doi.org/10.1016/j.quascirev.2016.05.027.

Simón, J.L., Arlegui, L.E., Ezquerro, L., Lafuente, P., Liesa, C.L., Luzón, A., 2017. Assessing interaction of active extensional faults from structural and paleoseismological analysis: the Teruel and Concud faults (eastern Spain). J. Struct. Geol. 103, 100–119. https://doi.org/10.1016/j.jsg.2017.08.003.

Simón, J.L., Arlegui, L.E., Ezquerro, L., Lafuente, P., Liesa, C.L., Luzón, A., 2016. Enhanced palaeoseismic succession at the Concud Fault (Iberian Chain, Spain): new insights for seismic hazard assessment. Nat. Hazards 80, 1967–1993. https://doi.org/10.1007/s11069-015-2054-6.

Simón, J.L., Arlegui, L.E., Lafuente, P., Liesa, C.L., 2012. Active extensional faults in the central-eastern Iberian Chain, Spain. J. Iber. Geol. 38, 127–144. https://doi.org/10.5209/rev_JIGE.2012.v38.n1.39209.

Simón, J.L., Ezquerro, L., Arlegui, L.E., Liesa, C.L., Luzón, A., Medialdea, A., García, A., Zarazaga, D., 2019. Role of transverse structures in paleoseismicity and drainage rearrangement in rift systems: the case of the Valdecebro fault zone (Teruel graben, eastern Spain). Int. J. Earth Sci. 108, 1429–1449. https://doi.org/10.1007/s00531-019-01707-9.

Simón, J.L., Lafuente, P., Arlegui, L.E., 2005. Caracterización paleosísmica preliminar de la falla de Concud (fosa del Jiloca, Teruel). Geogaceta 38, 63–66.

Simón, J.L., Pérez-Cueva, A.J., Calvo Cases, A., 2013. Tectonic beheading of fluvial valleys in the Maestrat grabens (eastern Spain): insights into slip rates of Pleistocene extensional faults. Tectonophysics 593, 73–84. https://doi.org/10.1016/j.tecto.2013.02.026.

Sowers, J.M., Noller, J.S., Lettis, W.R. (Eds.), 1998. Dating and Earthquakes: Review of Quaternary Geochronology and its Application to Paleoseismology (Washington, D. C).

Stevens, T., Buylaert, J.-P., Murray, A.S., 2009. Towards development of a broadly-applicable SAR TT-OSL dating protocol for quartz. Radiat. Meas. 44, 639–645. https://doi.org/10.1016/j.radmeas.2009.02.015.

Streig, A.R., Weldon II, R.J., Biasi, G., Dawson, T.E., Gavin, D.G., Guilderson, T.P., 2020. New insights into paleoseismic age models on the northern san Andreas Fault: charcoal inbuilt ages and updated earthquake correlations. Bull. Seismol. Soc. Am. XX, 1–13. https://doi.org/10.1785/0120190307.

Stuiver, M., Polach, H.A., 1977. Discussion reporting of ^{14}C data. Radiocarbon 19, 355–363. https://doi.org/10.1017/S0033822200003672.

Tissoux, H., Falguères, C., Voinchet, P., Toyoda, S., Bahain, J.J., Despriée, J., 2007. Potential use of Ti-center in ESR dating of fluvial sediment. Quat. Geochronol. 2, 367–372. https://doi.org/10.1016/j.quageo.2006.04.006.

Toker, E., 2017. Quaternary fluvial tufas of Sarıkavak area, southwestern Turkey: facies and depositional systems. Quat. Int. 437, 37–50. https://doi.org/10.1016/j.quaint.2016.06.034.

Toyoda, S., Falguères, C., 2003. The method to represent the ESR signal intensity of the aluminium hole center in quartz for the purpose of dating. Adv. ESR Appl. 20, 7–10.

Toyoda, S., Voinchet, P., Falguères, C., Dolo, J.M., Laurent, M., 2000. Bleaching of ESR signals by the sunlight: a laboratory experiment for establishing the ESR dating of sediments. Appl. Radiat. Isot. 52, 1357–1362. https://doi.org/10.1016/S0969-8043(00)00095-6.

Vandenberghe, D., De Corte, F., Buylaert, J.-P., Kučera, J., Van den haute, P., 2008. On the internal radioactivity in quartz. Radiat. Meas. 43, 771–775. https://doi.org/10.1016/j.radmeas.2008.01.016.

Voinchet, P., Falguères, C., Laurent, M., Toyoda, S., Bahain, J.J., Dolo, J.M., 2003. Artificial optical bleaching of the Aluminium center in quartz implications to ESR dating of sediments. Quat. Sci. Rev. 22, 1335–1338. https://doi.org/10.1016/S0277-3791(03)00062-3.

Wintle, A., 2008a. Fifty years of luminescence dating. Archaeometry 50, 276–312. https://doi.org/10.1111/j.1475-4754.2008.00392.x.

Wintle, A., 2008b. Luminescence dating: where it has been and where it is going. Boreas 37, 471–482. https://doi.org/10.1111/j.1502-3885.2008.00059.x.

Wintle, A., Huntley, D.J., 1982. Thermoluminescence dating of sediments. Quat. Sci. Rev. 1, 31–53.

Woda, C., Wagner, G.A., 2007. Non-monotonic dose dependence of the Ge- and Ti-centres in quartz. Radiat. Meas. 42, 1441–1452. https://doi.org/10.1016/j.radmeas.2007.03.003.

Yokoyama, Y., Falguères, C., Quaegebeur, J.P., 1985. ESR dating of quartz from Quaternary sediments: first attempt. Nucl. Tracks Radiat. Meas. 10, 921–928.

Young, R.R., Coppersmith, K.J., 1985. Implications of fault slip rates and earthquake recurrence models to probabilistic seismic hazard estimates. Bull. Seismol. Soc. Am. 75, 939–964.

Zimmerman, D.W., 1971. Thermoluminescence dating using fine grains from pottery. Archaeometry 13, 29–52. https://doi.org/10.1111/j.1475-4754.1971.tb00028.x.